CALIFORNIA
ENERGY COMMISSION

Energy Research and Development Division

FINAL PROJECT REPORT

High-Resolution Imaging of Geothermal Flow Paths Using a Cost-Effective Dense Seismic Network

Gavin Newsom, Governor

January 2021 | CEC-500-2021-004

PREPARED BY:

Primary Authors:
Dr. Roland Gritto
Dr. Seiji Nakajawa

Lawrence Berkeley National Laboratory
1 Cyclotron Road
Berkeley, CA 94720

Contract Number: EPC-16-021

PREPARED FOR:
California Energy Commission

Chuck Gentry
Project Manager

Jonah Steinbuck, Ph.D.
Office Manager
ENERGY GENERATION RESEARCH OFFICE

Laurie ten Hope
Deputy Director
ENERGY RESEARCH AND DEVELOPMENT DIVISION

Drew Bohan
Executive Director

ACKNOWLEDGEMENTS

The authors acknowledge the California Energy Commission (CEC) for financial assistance under contract EPC-16-021. The authors would like to thank Chuck Gentry (CEC contract manager) for his continued support during the project. The authors are grateful to Calpine Corporation for access to The Geysers geothermal field. Finally, the authors would like to thank Craig Hartline for providing reservoir data and numerous fruitful discussions on reservoir properties and on the interpretation of the seismic data as they relate to reservoir operations. Thanks are also extended to Ramsey Haught for his help in testing and installing the seismic recording systems, to Alex Morales, John Peterson and Ed Nichols (Lawrence Berkeley National Laboratory) for their help installing the seismic recording systems and to Martin Schoenball and Florian Soom (Lawrence Berkeley National Laboratory) for their help collecting the seismic field data.

PREFACE

The California Energy Commission's (CEC) Energy Research and Development Division supports energy research and development programs to spur innovation in energy efficiency, renewable energy and advanced clean generation, energy-related environmental protection, energy transmission and distribution and transportation.

In 2012, the Electric Program Investment Charge (EPIC) was established by the California Public Utilities Commission to fund public investments in research to create and advance new energy solutions, foster regional innovation and bring ideas from the lab to the marketplace. The CEC and the state's three largest investor-owned utilities—Pacific Gas and Electric Company, San Diego Gas & Electric Company and Southern California Edison Company—were selected to administer the EPIC funds and advance novel technologies, tools, and strategies that provide benefits to their electric ratepayers.

The CEC is committed to ensuring public participation in its research and development programs that promote greater reliability, lower costs, and increase safety for the California electric ratepayer and include:

- Providing societal benefits.
- Reducing greenhouse gas emission in the electricity sector at the lowest possible cost.
- Supporting California's loading order to meet energy needs first with energy efficiency and demand response, next with renewable energy (distributed generation and utility scale), and finally with clean, conventional electricity supply.
- Supporting low-emission vehicles and transportation.
- Providing economic development.
- Using ratepayer funds efficiently.

High-Resolution Imaging of Geothermal Flow Paths Using a Cost-Effective Dense Seismic Network is the final report for project EPC-16-021 conducted by the Lawrence Berkeley National Laboratory. The information from this project contributes to the Energy Research and Development Division's EPIC Program.

For more information about the Energy Research and Development Division, please visit the CEC's research website (www.energy.ca.gov/research/) or contact the CEC at 916-327-1551.

ABSTRACT

This project successfully developed an advanced, low-cost, automated seismic imaging system that used small earthquakes to form high-resolution images of underground distributions of steam and water flow paths in producing geothermal fields, and demonstrated the practical implementation of this technology in an operating geothermal field. The project advanced the technology by integrating the components into a system that can be cost-effectively, reliably, and routinely used in operating geothermal fields to provide images of the movement of fluids in space with a fast-turnaround time from data collection to processing, imaging, and rock physics interpretations. The project demonstrated the technology at The Geysers geothermal reservoir in northern California, where a 91-station low-cost seismic network was installed over a 5 x 5 kilometer study area. The project team acquired and processed seismic data from more than 17,000 micro-seismic events and generated images of seismic velocities representing reservoir flow paths. Correlation of the seismic velocities with known water injection and steam production volumes allowed the team to calibrate the seismic data, which can now be applied throughout the reservoir where borehole data are unavailable. The seismic velocities and resulting calculated rock properties, together with reservoir data derived from observations in boreholes, allow interpretation of the seismic images to identify water and steam saturated zones, fluid pathways, and fractured or solid rock. This information allows the reservoir operator to develop a better drilling program that minimizes drilling of unsuccessful wells, resulting in reduced costs and lower electricity rates for California ratepayers.

Keywords: Micro-seismicity, cost-effective dense seismic networks, high resolution seismic imaging, delineation of production zones

Please use the following citation for this report:

Nakagawa, Seiji and Roland Gritto. 2021. *High-Resolution Imaging of Geothermal Flow Paths Using a Cost-Effective Dense Seismic Network*. California Energy Commission. Publication Number: CEC-500-2021-004.

TABLE OF CONTENTS

LIST OF FIGURES

Page

LIST OF TABLES

Page

EXECUTIVE SUMMARY

Introduction

California Senate Bill 100 established a statewide goal of 60 percent electricity generation from renewable sources by 2030. Continued growth of California's broad portfolio of renewable energy, including geothermal, is required to achieve the goals of SB 100. However, a major barrier to achieving the state's mandated renewable electricity targets is that fluctuating resources like wind and solar require complementary resources and strategies to ensure grid reliability. Geothermal energy, a virtually untapped energy resource derived from the Earth's heat, is a key complementary resource, which is independent of external weather conditions and provides clean, renewable power around the clock, emits little or no greenhouse gases, and takes a very small environmental footprint to develop.

Over the years, state and federal agencies have helped develop, demonstrate, and install innovative technologies to stimulate the growth of the geothermal industry within the renewable energy sector and encourage quick adoption of these technologies by the public and private sectors. Geothermal energy resource development relies on boreholes that tap the Earth's heat. This heat is brought to the surface in the form of hot water or steam and drives turbines that generate electricity.

Geothermal boreholes can cost as much as $6.5 million and providing reliable information on the drilling target at depth reduces the risk of a dry or unsuccessful well. However, determining exactly where to place geothermal wells is not trivial. To address this concern, this project developed a seismic imaging technology that provides high-resolution images of the structure of the Earth's crust in the geothermal reservoir, including the location of hot water and steam, to help geothermal operators decide where to successfully situate boreholes. Seismic imaging uses recordings of ground vibrations in the Earth generated either by small explosive sources or, as in this project, by small earthquakes. The technology subsequently transforms those ground vibrations into images of the subsurface to provide insight into the structure of the Earth. Seismic imaging is a mature technology that is successfully applied in the oil and gas industry, but structural variations seen in geothermal reservoirs are very different from the kinds of sedimentary structures in typical oil and gas reservoirs. Therefore, the technology developed for the oil and gas industry cannot be easily transferred to geothermal reservoirs. While companies developed new seismic imaging methods in the recent past to address these shortcomings, those methods are labor intensive and most lack the level of detail required for reliable and accurate placement of boreholes.

Project Purpose

In this project, the research team developed a semi-automatic and near real-time technology to perform high-resolution seismic imaging of geothermal reservoirs to show the geological, tectonic, and hydrological structure of the reservoirs and support operators' borehole planning programs. The primary purposes of this project were to (1) develop an advanced, low-cost, automated seismic imaging system that uses small earthquakes to form high-resolution images of subsurface fluid flow, flow barriers, and reservoir structure in producing geothermal fields, and (2) demonstrate the practical implementation of this technology in an operating geothermal field. The technical advancement of this project is the integration of these

components into a system that can be cost-effectively, reliably and routinely deployed in operating geothermal fields to map the movement of fluids in space and time with a fast-turnaround time from data collection to processing, imaging, and rock physics interpretations. Unlike similar commercially available systems for monitoring hydrofractures in oil and gas reservoirs, this effort focuses on micro-earthquake imaging challenges unique to geothermal reservoirs, such as complex fracturing, faulting, and diverse compositions of rock. The product of this project will enable geothermal operators to carry out their operations more efficiently by drilling productive wells, avoiding drilling hazards, and optimizing production. Better control of borehole placement will reduce operator losses due to dry or unproductive wells, translating into lower electricity rates for California electricity ratepayers.

Project Approach

The research team consisted of researchers from the Lawrence Berkeley National Laboratory (LBNL), Array Information Technology (AIT), Jarpe Data Solutions (JDS), and Calpine Corporation (the operator of The Geysers geothermal field in northern California where the developed technology was applied). The technology included the following:

- Development and engineering of low-cost seismic ground vibration sensors.
- Design of a seismic network able to detect small-scale structures at depth.
- Development of software to automatically process seismic data.
- Advancement of software to generate images of the geothermal reservoir structure using the processed seismic data.
- Technology that maps the seismic imaging results to reservoir properties so the geothermal operator can use the results to support its drilling program.

JDS designed and engineered the low-cost seismic vibration sensors, which are conceived to operate independently at geothermal reservoirs. The sensors include an internal battery and solar panel to supply power, a Global Positioning System (GPS) antenna for location accuracy and timing, a three-component ground motion sensor, a 24-bit analog-to-digital converter, and memory cards for data storage. The technical features of the sensors helped overcome limitations inherent to the steep land surfaces and vegetation coverage at The Geysers that prevent continuous exposure to sunlight and GPS satellite signals. The combination of solar panels and internal batteries provided two to three weeks of continuous operation in case of overcast weather conditions or dark skies. The electronic circuit boards were designed to automatically turn off and on when battery power reached a predetermined level.

One of the goals of the project was improving the ability of the technology to detect the small-scale structure of the reservoir by increasing the number of seismic sensors and optimizing their placement in the field. The design of the high-resolution network included a numerical study that analyzed the placement of 100 seismic stations spaced in regular and irregular geometry in a 5 x 5 kilometer study area chosen by Calpine Corp. to support its future development program in the region. The measure of network performance is the ability to separate the measurements of seismic wave propagation velocities between two closely spaced points in the reservoir. The steep terrain in the study area and the thick vegetation prevented deployment of a regularly spaced 10 x 10 seismic sensor network. However, the results of the network design study showed negligible differences between a regularly and

randomly spaced 100 station network for a 5 x 5 kilometer area. Nevertheless, the researchers installed a semi-regularly spaced network with 91 seismic stations to demonstrate the technology in early 2018 that has been operating ever since.

LBNL and JDS had previously developed software to automatically process the recorded data for seismic wave arrival times and seismic wave amplitudes. In this project, the project team further developed the software using a combination of techniques based on artificial intelligence and improved the detection of seismic signals in noisy conditions. Operating geothermal reservoirs, such as The Geysers, are known for adverse noise conditions because proximity to power plants, cooling towers, and pipelines with flowing water and steam generates ground motions that interfere with recorded seismic signals from small earthquakes.

The researchers had to modify the software codes which convert the seismic data to images of reservoir structure to account for the high number of (1) earthquakes that occur in The Geysers, (2) the high number of seismic vibration sensors, and (3) small volumes (150 x 150 x 150 meters) into which the 5 x 5 x 5 kilometers reservoir volume was subdivided. After modification, the software codes calculated the propagation velocities of the seismic waves for each of the small volumes to provide an image of the reservoir structure. The project team accomplished the software modifications by changing the memory structure of the software codes (adding dynamic memory allocation) and adding software that can efficiently and rapidly model the seismic wave propagation through the reservoir. Consequently, the revised software codes could handle the vast volume of seismic data generated at The Geysers geothermal reservoir.

The research team processed and inverted the seismic data to generate three-dimensional (3D) images of seismic wave propagation velocities in the reservoir. The team also converted the seismic velocities to rock properties to provide geomechanical parameters for the correlation to reservoir properties. Researchers then incorporated the 3D data volumes into The Geysers 3D reservoir model for correlation analyses with geological, tectonic, and hydrological structure. These analyses provided the support for Calpine's current drilling program.

Researchers established several technical performance metrics for various project tasks, including:

- Resolution of velocity estimates to appraise the performance of the network.
- Evaluation of the seismic sensor performance including operation time.
- Estimates of the earthquake location error.
- Spatial correlation of the seismic imaging results to geological, tectonic, and hydrological structure in the 3D geothermal reservoir model.

The project team formed a technical advisory committee composed of five experts from academia, national laboratories, and industry. The committee included Professor Douglas Dreger (University of California, Berkeley), Dr. Ernest Majer (LBNL), Professor Lane Johnson (LBNL), Dr. Brian Bonner (LBNL), and Mr. Craig Hartline (Calpine Corp.). The researchers convened two committee meetings during the first two years of the project. Overall, the members of the committee were pleased with the planning, operation, and management of the project and discussions focused mainly on technical issues regarding seismic wave

propagation in geothermal reservoirs. Committee recommendations incorporated into the project included: (1) co-location of low-cost seismic sensors with permanently installed seismic sensors (five sensors were co-located in the study area); (2) rotation of the three-component sensor to separate the seismic P-wave and S-wave signals (incorporated into the data processing software); and (3) recording and storing continuous seismic data for future research projects (the continuously recorded data were stored and are available for future research projects).

Project Results

The research team built the low-cost seismic vibration sensors to the desired technical specifications and cost. The network design showed that using 100 seismic sensors in the 5 x 5 kilometer study area resulted in negligible differences in resolution of the seismic network based on sensor locations (for example, regular versus random). This result was unexpected and will prove useful for future dense-station networks.

The demonstration of the technology in the field proved successful. The technology detected and analyzed more than 17,000 earthquakes, yielding high-resolution images of the complex structure of the reservoir that showed regions with high concentrations of steam and water. While regions with high steam concentrations are targets for future production wells, knowing the location of water-saturated zones is also useful to drill complementary injection wells to optimally distribute water in the reservoir. In contrast, the researchers found that seismically derived images of regions known to Calpine to be unproductive showed a high degree of intact rock that inhibited flow of water or steam throughout the reservoir. Finally, the team found that the locations of fractures and faults in the 3D reservoir model coincided with boundaries dividing regions with different wave propagation velocities derived from the seismic data. This proved that the seismic results match the structure of the 3D reservoir model.

Information contained in Calpine's 3D reservoir model corroborated most of the results of the 3D seismic imaging. As such, the project demonstrated the successful application of the technology in an operational geothermal reservoir. In general, the technology is applicable to any reservoir where natural seismicity is observed. However, because geothermal reservoirs generate a great deal of seismicity by injecting cold water into hot rock, the technology applies particularly to imaging the structure of geothermal reservoirs.

The size (magnitude) of earthquakes in geothermal reservoirs is typically low. The low magnitude combined with noise from an operating geothermal reservoir make it difficult to detect and locate small earthquakes, particularly at longer distances from the seismic stations. Therefore, seismic vibration sensors with higher fidelity and broader spectral sensitivity are advantageous for future applications. While these kinds of sensors are more expensive, advances in technology will be bringing costs down in the future. Telemetered seismic data transmission is imperative for real-time monitoring. The seismic recorders used in this project have the option to include cell phone boards for automatic data transmission. However, because cell phone reception at The Geysers geothermal reservoir is extremely poor, automatic data transmission was not implemented and the data were recovered quarterly.

Technology Transfer

The research team reported project results at scientific conferences during the project and presented five papers, two at the Stanford Geothermal Workshop and three at the American Geophysical Union Annual Meeting.

The immediate results of the project are being used by Calpine Corp., the operator of The Geysers geothermal reservoir, to inform its drilling program in the study area. The program envisions the drilling of new wells and the reopening and deepening of abandoned wells to improve production in the area.

The near-term market of the developed technology is its application to The Geysers, where the deployed seismic network is still operating. Calpine has already indicated willingness to maintain the network and continue future operations. Calpine has incorporated the derived 3D models of seismic propagation velocity and elastic rock parameters into its 3D reservoir model and will use those models to guide drilling operations in the future.

Mid-term target markets include geothermal reservoirs in California, including the Coso and Salton Sea geothermal fields. These fields reveal induced seismicity that can be used to perform the seismic imaging conducted in this project. Long-term markets for this technology include geothermal reservoirs outside of California such as new developments in Cascadia (northwestern United States), Nevada, Idaho, Utah, and Hawaii where planned enhanced geothermal systems are expected to generate induced seismicity. Additionally, international markets may include geothermally productive regions such as Iceland, Turkey, Taiwan, the Philippines, Indonesia, and New Zealand.

JDS co-developed the technology and offers the service to operators in California, the United States, and abroad. JDS will continue to market this technology. During the presentations of the results at scientific conferences, several stakeholders approached the research team who were interested in using the low-cost seismic vibration sensors for their geothermal operations.

The successful application of this technology at The Geysers has already resulted in Calpine Corp. embracing the results of the project to inform planning of its drilling program. This is an important first step that proves seismic imaging can be used to improve reservoir operations. JDS can also use examples of the results to promote the technology to other stakeholders.

Enhanced geothermal systems can be difficult to manage because knowledge of the generated fracture network relies on the availability of remote sensing techniques. By proving this technology can provide accurate and detailed images of the processes and heterogeneity in a geothermal reservoir, governmental agencies and public regulators may be more likely to promote the development of those systems.

At present, the developed technology is being coupled with magneto telluric sounding, another geophysical imaging technique, to improve the reliability of the resulting images of the reservoir structure.

Benefits to California

The results of the current project will benefit California ratepayers because they allow Calpine Corp. to optimize reservoir operations at The Geysers geothermal reservoir, which provides around 850 megawatts of electricity to ratepayers in northern California.

Project results will also improve Calpine Corp.'s drilling program, resulting in reduced costs and lower electricity rates for California ratepayers. For example, in the project study area, a recently drilled production well turned out dry and was subsequently converted to a water injection well. Situations like this increase the total cost of Calpine's drilling program without generating additional electricity. After results from the developed technology became available, they were incorporated in the geothermal reservoir model and have already aided in the planning of future wells. The cost of a geothermal well can be as high as $6.5 million, so assistance with successful completion of the production and water injection wells will reduce the overall cost of drilling. A 5 percent to 10 percent improvement in steam recovery and water injection efficiency is realistic based on the results of this project. If this project improves efficiency by 5 percent, the annual savings at The Geysers would amount to $560,000. An improvement of 10 percent would provide annual savings of $825,000. These figures include the savings in purchasing and operating the low-cost seismic network over similar competitive networks at $280,000/year. While the developed technology can be successfully operated as a stand-alone tool, a new research project is currently further refining the technology by coupling it with magneto telluric sounding, another geophysical imaging technique, to improve the reliability of the resulting images of the reservoir structure.

CHAPTER 1: Introduction

Background

In contrast to weather-dependent renewable resources such as solar and wind, geothermal energy is a virtually untapped energy resource derived from the Earth's heat that provides clean, renewable power around the clock, emits little or no greenhouse gases, and takes a very small environmental footprint to develop. By developing, demonstrating, and deploying innovative technologies, the U.S. Department of Energy (USDOE) Geothermal Technology Office's (GTO) efforts are helping to stimulate the growth of the geothermal industry within the renewable energy sector and encouraging quick adoption of technologies by the public and private sectors.

Development of geothermal energy resources relies on boreholes that tap the heat at depth. This heat is brought to the surface in the form of hot water or hot steam that drives turbines to produce electricity. However, knowing the exact location to site geothermal wells is non-trivial. This project developed seismic imaging technology to provide high-resolution images of the tectonic structure of the geothermal reservoir, including the location of hot water and steam, which will support the siting of boreholes by geothermal operators.

Seismic imaging is a mature technology that has been successfully applied in the oil and gas industry. However, typical hydrocarbon reservoirs are located in layered sedimentary basins that do not exhibit the structural heterogeneity encountered in geothermal reservoirs. Therefore, the technology that has been developed for the oil and gas industry cannot be easily transferred to geothermal reservoirs. In the recent past, new seismic imaging methods have been developed to address these shortcomings. However, these methods are labor intensive and most lack the resolution required for reliable and accurate siting of boreholes. Therefore, in this project the research team developed a semi-automatic and near-real time technology to perform high-resolution seismic imaging of geothermal reservoirs to image the geological, tectonic, and hydrological structure of the reservoir and to support operators with their borehole planning program.

Specifically, the primary goals of this project were: (1) to develop an advanced, low-cost, automated tomographic imaging system that uses micro-earthquakes to form high spatial and temporal resolution images of subsurface fluid flow, flow barriers and heterogeneity in producing geothermal fields; and (2) to demonstrate the practical implementation of this technology in an operating geothermal field. The technical advancement of this project is the integration of these components into a system that can be cost-effectively, reliably and routinely deployed in operating geothermal fields to image the movement of fluids in space and time with a fast-turnaround time from data collection, to processing, to imaging, and to rock physics interpretations. Unlike similar systems that are commercially available for monitoring hydrofractures in oil and gas reservoirs, this effort focuses on micro-earthquake imaging challenges that are unique to geothermal reservoirs, which can include complex fracturing and faulting, heterogeneous overburden and limited seismic velocity control. The product of this project will enable geothermal operators to carry out their operations more

efficiently, including drilling productive wells, avoiding drilling hazards, and optimizing production. Geothermal boreholes can cost as much as $6.5 million and providing reliable information on the drilling target at depth reduces the risk of a dry or unsuccessful well.

The project team undertook development and demonstration of the proposed technology at The Geysers geothermal reservoir in northern California. The Geysers geothermal reservoir, extending over an area of ~115 square kilometers (km^2) in the Mayacamas Mountains of Northern California, is the largest geothermal reservoir in the world with approximately 1.6 gigawatts (GW) installed electric capacity and current production of about 850 megawatts (MW). Operations at The Geysers, a steam dominated reservoir, commenced in the 1960s and have included the reinjection of condensates, rain, and nearby creek water since the early 1970s to improve steam pressure in the reservoir. These operations were supplemented in recent years by injection of treated wastewater from nearby communities to sustain the production of the geothermal resource. The South East Geysers Effluent Project (SEGEP), a 46-km long pipeline from Lake County delivering 22 million liters (l)/day, was commissioned in 1998 to resupply the South East Geysers with water, while a second 64-km long pipeline from Santa Rosa, the Santa Rosa Geysers Recharge Project (SRGRP), delivering 41 million l/day, was commissioned in 2003 (Majer and Peterson, 2007). Figure 1 shows the location of The Geysers geothermal reservoir in northern California relative to the cities of Santa Rosa and San Francisco.

Figure 1: Location of The Geysers Geothermal Reservoir

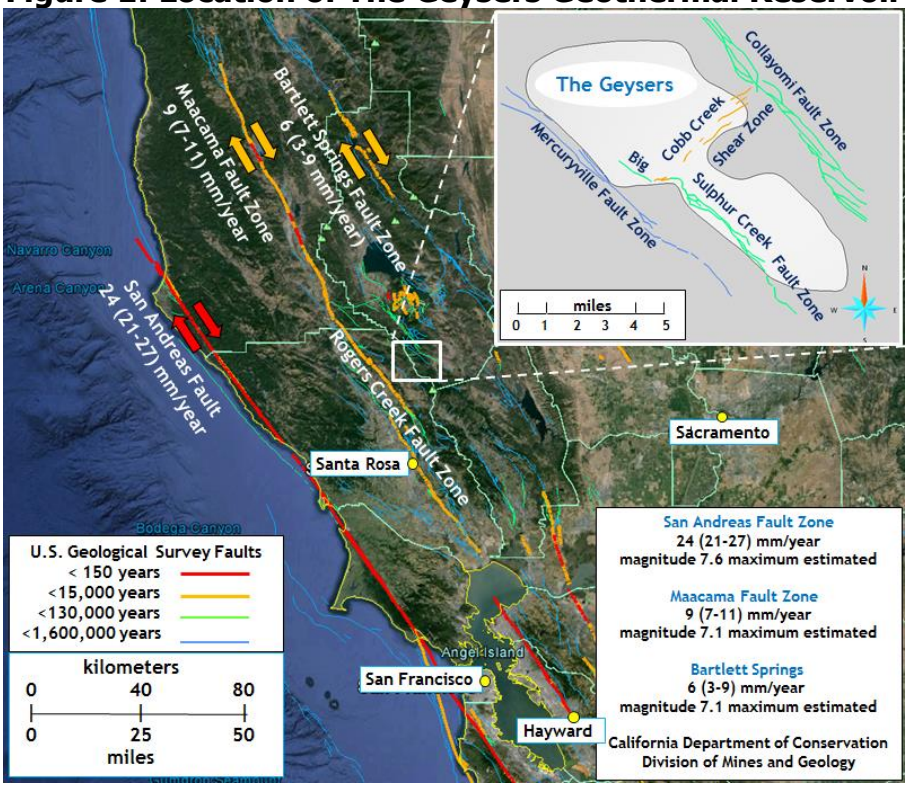

The San Andreas Fault System, including the Maacama / Rodgers Creek Fault Zone and Bartlett Spring Fault Zone. United States Geological Survey Faults with activity in the past 1.6 million years are displayed. Primary bounding fault zones are shown in the inset at upper right. This Google Earth image includes fault parameters from the California Division of Mines and Geology, 1996 (from Hartline, 2016).

Source: Google Earth

While wastewater injection has successfully replenished the resource and the steam production that was in severe decline during the late 1980s, it has also been linked to elevated rates of micro-seismicity in the reservoir when compared to regional rates (Ludwin et al., 1982). The seismicity has been found to occur on either set of orthogonal faults in northwest and northeast directions and is used to delineate the geometry of faulting in the reservoir to support reservoir operations. The orthogonal faulting encountered in The Geysers results in compartmentation of blocks throughout the reservoir. Where faults are impermeable and located close to water injection wells, fluid-flow radially from the borehole is impeded because the faults act as barriers. In these cases, fluid-flow occurs along fault strike and the injected water volume often resides within the compartment formed by the faults. This complicates the siting of production wells targeting the injected water, particularly when the locations of faults are unknown. Therefore, past efforts have used micro-seismic hypocenter locations to delineate fluid flow through the reservoir. However, this technique is not unique because not all seismicity in the reservoir is associated with the presence of fluid-flow (Gritto et al., 2016; Dreger et al., 2018). In contrast, seismic tomographic imaging of the P- and S-wave velocities can be used to determine the presence and the location of fluids in the reservoir (Gritto et al., 2013a; Gritto et al., 2013b). However, for this technique to be successful, the spatial resolution of the velocity estimates need to be sufficiently high to image the reservoir with high fidelity. Additionally, rock-physics transforms and effective medium theory (Mavko et al., 1998) need to be employed to convert the seismic velocities to fluid properties and to parameters such as reservoir pressure, which can aid geothermal operators to understand fluid-flow and the locations of flow barriers, to evaluate the heterogeneity of the reservoir, as well as to estimate the temporal changes during operations. This knowledge will enable more efficient operations, including drilling productive wells, avoiding drilling hazards, and optimizing production. Because tomographic imaging techniques still need improvement to achieve the above stated goals, the current project is designed to address these shortcomings.

Objectives of Fluid Imaging

For more than 30 years, a USDOE GTO-funded seismic network operated by Lawrence Berkeley National Laboratory (LBNL) has been recording seismicity at The Geysers. At present, the network consists of 34 stations covering an area of ~100 km^2 with a station density of 0.3 stations/km^2. The recorded seismicity is regularly analyzed for hypocenter locations and moment magnitudes and provided to Calpine in support of reservoir operations. The micro-earthquake locations and magnitudes are uploaded into Calpine's earth modeling software to support the development of The Geysers' three-dimensional (3D) structural model. The constraints of this model are provided by approximately 870 lithology logs, surface geology maps, reservoir temperature and pressure, tracer analysis patterns, heat flow patterns, reservoir history matching, noncondensable gas concentrations and seismicity hypocenter databases provided by the Northern California Earthquake Data Center (NCEDC) and LBNL (Hartline et al., 2015; 2016; 2019). At The Geysers, micro-seismicity is believed to be triggered by slip along the faces of preexisting fractures and faults due to thermal contraction of the rock by the injected cold water as it moves through the hot, dry fractured rock mass. Thus, this type of micro-fracturing is used as a proxy for the presence of water (Figure 2a). Analyses of these induced seismicity patterns have provided Calpine a better understanding of the complex (inactive) fault zones and fracture systems existing throughout The Geysers. However, Calpine has also observed that micro-earthquake locations are not a direct proxy for

fluid-flow when fluid moves along permeable fractures or faults without triggering micro-seismicity (Figure 2b).

Figure 2: Map Views of Micro-Earthquakes at The Geysers

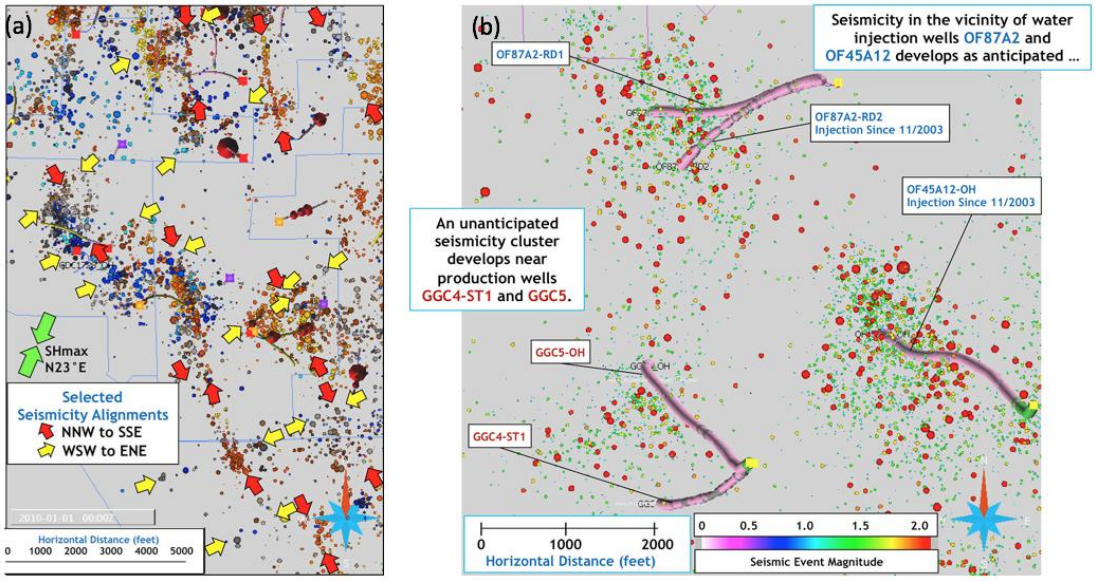

Map views of micro-earthquakes at The Geysers for a seven-year period (2003-2009) and a depth range of 915 m to 2440 m. (a) Alignment of micro-seismicity along quasi-orthogonal, vertical planes indicates relict shear zones (red arrows) and trans-tensional fault zones (yellow arrows). (b) Pre-drilling analysis of seismicity reveals expected characteristic low-magnitude micro-earthquakes in the vicinity of injection wells (wells at top-center and lower-right), indicative of flow paths and flow barriers, and an unanticipated, well–contained cluster of micro-earthquakes in the vicinity of two shut-in production wells GGC4-ST1 and GGC5-OH (wells at bottom-left) (from Hartline et al., 2015).

Source: Lawrence Berkeley National Laboratory

Calpine's 3D predrilling analyses and detailed 3D fracture zone interpretations indicated the potential to use induced seismic event patterns and progressions, including those seen on synchronized water injection and induced seismicity animations, as a significant constraint on Geysers 3D structural model development. Induced seismicity patterns and seismic event density variations appear to indicate permeability variations and resulting fluid flow, allowing the interpretation of fracture zones and lithological changes. For example, the transition from Hornfelsic Graywacke to Felsite generally correlates with a decrease in seismic event density in the west-central and southeast Geysers (Hartline et al., 2016). The fact that the Top Felsite markers, based on drilling information, and the seismic event density transition are spatially consistent increases Calpine's confidence in the use of seismic event hypocenters as an additional constraint on Top Felsite surface development and 3D structural model development in general (Hartline et al., 2016; 2019). In addition to the fracture zone interpretations, induced seismicity patterns were used to interpret the Big Sulphur Creek Fault Zone and the Mercuryville Fault Zone as series of anastomosing faults that essentially form the productive boundary of the Geysers' geothermal reservoir to the southwest (Hartline et al., 2016). The model development has generated a complex 3D model of the reservoir with four major subhorizontal interfaces consisting of top of steam, top of Hornfels Graywacke, top of Felsite and base of steam. These interfaces are intersected by a network of subvertical and subhorizontal faults that dissect the reservoir in northwest and northeast direction.

Figure 3 presents a section of the 3D model that falls within the 5 x 5 km study area of the current project.

Figure 3: 3D Views the Study Area with Faults and Major Interfaces

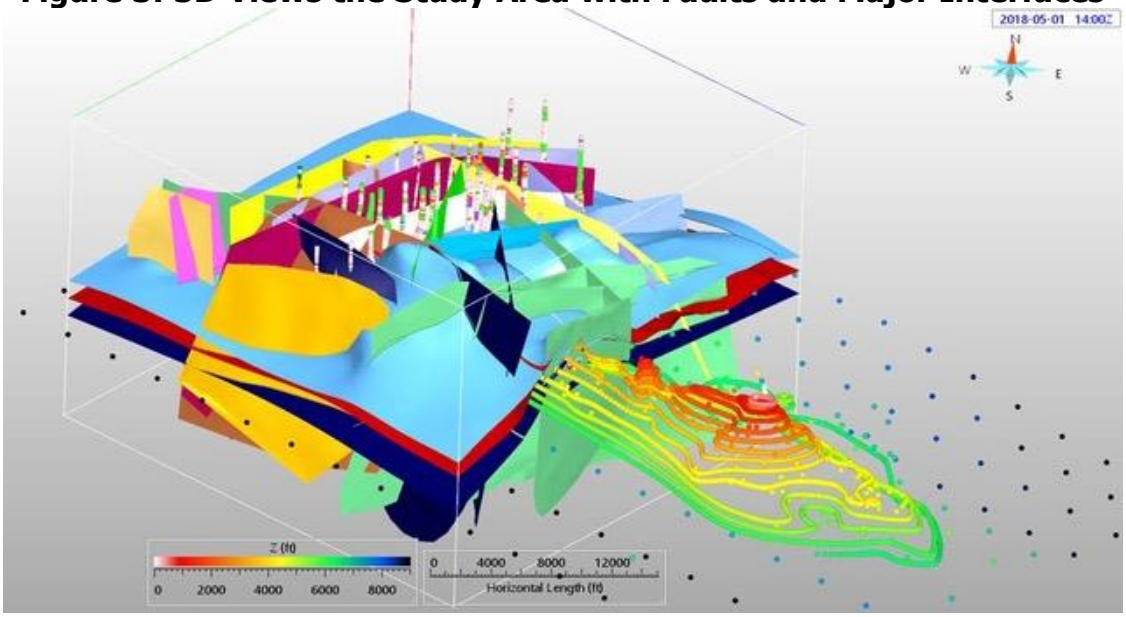

Three-dimensional view of the 5x5 km study area with horizontal interfaces and subvertical faults denoting the compartmentation of the reservoir. The feature indicated by the isosurfaces, protruding from the model in southeast direction, denotes the top of the Felsite horizon.

Source: Lawrence Berkeley National Laboratory

While the faults in Figure 3 are partly obscured by the interfaces, the image in Figure 4 displays the faults only. The figure demonstrates the high density and complexity of faulting throughout the reservoir, which is a consequence of The Geysers' location within the San Andreas transform fault system.

Figure 4: Map View of the Study Area with Faults

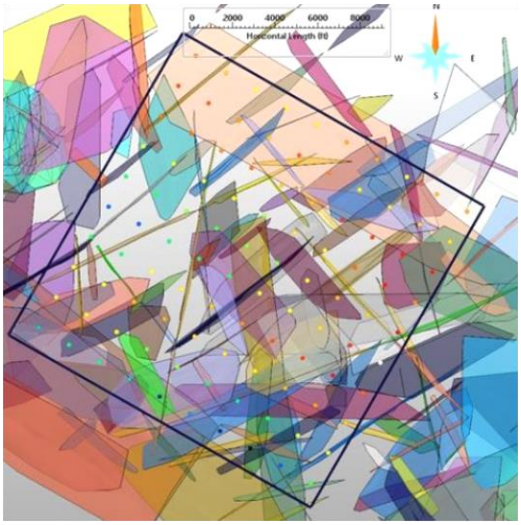

Map view of the 5 x 5 km study area (black square) with subvertical and subhorizontal faults crossing the region.

Source: Lawrence Berkeley National Laboratory

Considering that most of the fault geometries presented in the 3D models in Figure 3 and Figure 4 were derived from hypocenter locations obtained with the 34-station permanent seismic network mentioned above, it is easy to project the improvements achievable with the 91-station dense seismic temporary network that is the centerpiece of the current project. As presented in Chapter 2, the dense 91-station seismic network covers an area of 25 km^2 resulting in a station density of 3.6 stations/km^2, more than 10 times that of the permanent Geysers' network. The researchers anticipate that the high station density will result in an increase in event detection, due to shorter earthquake-station distances resulting in a decrease of the smallest detectable magnitude. The higher number of stations will also increase the number of seismic phase detections per event resulting in higher accuracy of hypocenter locations. Hypocenters with higher accuracy will improve the delineation of the fault geometries in the 3D structural model. At the same time, the increase in phase arrival times will improve the resolution of the tomographic images of the reservoir as demonstrated in Chapter 3. The increase in resolution of the tomographic images will yield improved estimates for the delineation of fluid pathways in the reservoir. The above-mentioned advantages of the dense seismic network will culminate in an improved 3D structural model of the geothermal reservoir.

CHAPTER 2:
Project Approach

The research team consisted of researchers from LBNL, Array Information Technology (AIT), Jarpe Data Solutions (JDS), and Calpine Corporation as the operator of The Geysers geothermal field in northern California where the developed technology is applied. The technology consisted of multiple parts, including the development and engineering of low-cost seismic sensors, the design of a high-resolution seismic network, the development of automatic seismic data processing software, the field demonstration of the seismic network, the advancement of software that generates images of the reservoir heterogeneity using the processed seismic data, and a technology that correlates the seismic imaging results to reservoir properties, such that the geothermal operator can use the results to support their drilling program.

Development and Engineering of Low-Cost Seismic Stations

The low-cost seismic stations, designed by JDS, have been used in the past for passive seismic monitoring in geothermal and seismic hazard applications. However, none of the past applications lasted as long as the planned multiyear operation in this project, which required improvement in the robustness of the design and in the power consumption of the electronic components. The researchers based the first tested station on an existing design, housed in a 25 x 25 x 10 centimeter (cm) box with a tilting solar panel as shown in Figure 5a. A concrete pad connected the stations to the ground (Figure 5a), while ground surfaces such as rock outcrops (Figure 5b, foreground) and soil (Figure 5b, background) were considered.

Figure 5: First-Generation Seismic Station

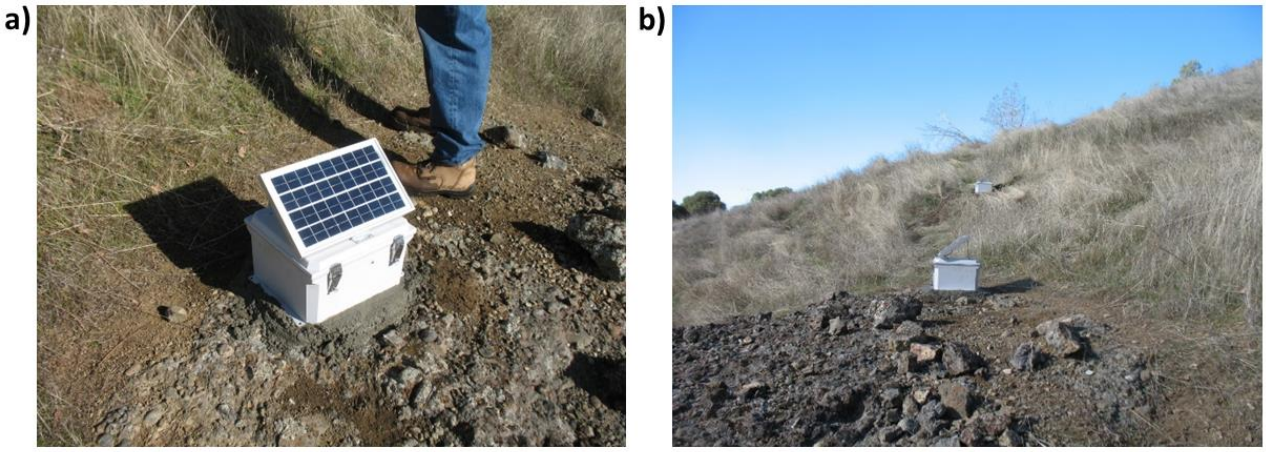

(a) First-generation seismic station deployed for quality testing at The Geysers. (b) Deployment on rock outcrop (foreground) and on soil (background).

Source: Lawrence Berkeley National Laboratory

The interior of the station comprises a 12-volt (V) battery, an electric circuit board, three orthogonally oriented 4.5 Hertz (Hz) geophones and a GPS antenna (Figure 6a). Six first-generation station were deployed at The Geysers, three of which were co-located with existing

permanent seismic station to test their performance. The deployment lasted one month, after which the stations were collected, and their performance evaluated. The interior of one station, shown in Figure 6a, revealed water damage to the circuit board that resulted in the decision to replace the station housing with a more rugged box with improved waterproofing.

Figure 6: Interior of First-Generation Seismic Station

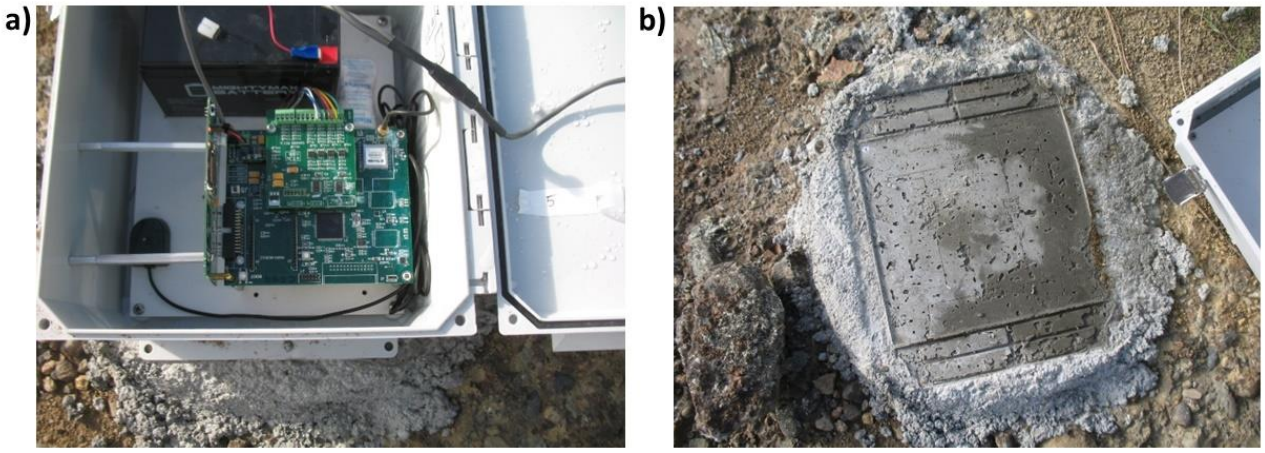

(a) Interior of first-generation seismic station revealing the electric circuit board, the battery, and the GPS antenna. The three orthogonal geophone components are arranged at the base of the box below the circuit board. (b) Concrete pad after station removal.

Source: Lawrence Berkeley National Laboratory

The conclusions of the first deployment resulted in the development of the second-generation seismic station, which included improved electronic components that required less power and a watertight enclosure. However, unexpected damage to the circuit boards during shipping and observed resonances during huddle testing resulted in the design of the third-generation seismic station including a one-piece metal bracket to better secure the electronic board and the decision to add metal fins to the outside of the box to improve coupling to the concrete pad and to avoid resonances. Figure 7 shows the design of the third-generation seismic station and its components. Figure 7a shows the 12-V battery next to the electronic circuit board. At the top of the circuit board, two slots for SD memory cards are visible as well as the GPS antenna cable. Three orthogonally oriented 4.5 Hz geophone components are mounted to the metal bracket below the circuit board (Figure 7b), while the metal fins are connected to the outside of the enclosure (Figure 7c) and extend into the concrete pad for improved coupling as shown in Figure 7d. The physical properties of the second- and third-generation stations are summarized in Table 1.

Figure 7: Third-Generation Seismic Station Components

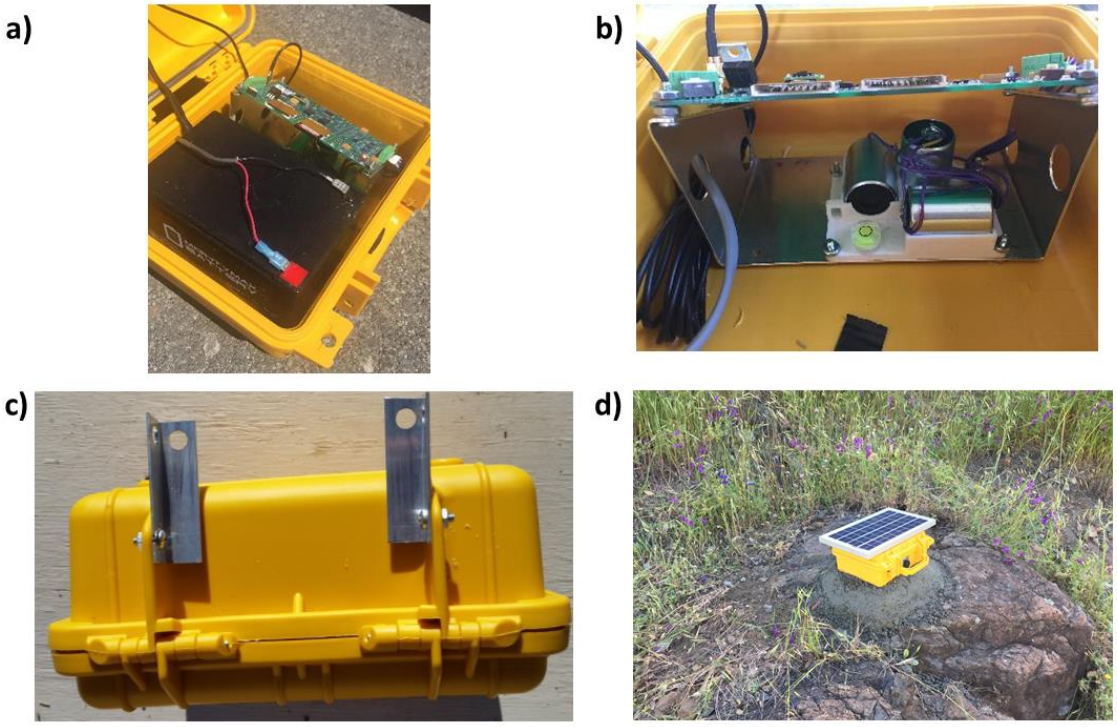

(a) Interior of third-generation seismic station with battery and electronic circuit board. (b) One-piece metal bracket with electronic circuit board (top) and three orthogonally oriented geophone components (bottom). (c) Metal fins attached to outside of watertight enclosure to improve coupling to concrete pad. (d) Station installed on a rock outcrop.

Source: Lawrence Berkeley National Laboratory

Table 1: Physical Properties of 2nd and 3rd Generation Low-Cost Seismic Station

Property	Value
Size	25x25x10 cm
Weight	4 kg
Input Voltage	10-16 VDC
Solar Panel	10 W, Not Tilting
Power Consumption	360 mW
Sensors	4.5 Hz, HGS, HG6-HS
Data Conversion	Delta-sigma, 24 Bit
Number of Channels	3
Sample Rate	200 sps (f_{NY} = 100 Hz)
Time Base	GPS (Internal Antenna)
GPS Accuracy	1 ms
Recording	Continuous
Output	SD Memory Card, 2 slots
Enclosure	Watertight*
Coupling	Concrete and Metal Fins (3rd generation only)

Source: Lawrence Berkeley National Laboratory

Design and Deployment of High-Resolution Seismic Network

The goal of this task was to conduct a network design study to determine the best placement of seismic stations to achieve optimum resolution of the estimates in reservoir parameters. The design study employed 100 sensors and analyzed the resulting resolution in elastic parameters such as P- and S-wave velocity estimates. The study was based on previously acquired micro-earthquake locations within the 5 km by 5 km study area, 3D P- and S-wave velocity models (Gritto et al, 2013a), surface topography, and site access information from Calpine. Earthquake locations were taken from the 2016 LBNL seismic catalog for The Geysers to obtain a representative one-year distribution of seismicity in the study region. A one-year distribution of seismicity is important, because the number of earthquakes depends on the volume of injected water, which is a function of seasonal availability. A total of 3,389 earthquakes were selected, with a maximum hypocenter depth of 4.5 km, as that was the resolution limit of the 3D P- and S-wave velocity models (Gritto et al., 2013a). The events are densely distributed and cluster in various locations of the region.

The researchers investigated network designs that included configurations with planar station locations and stations at elevations that matched the surface topography at The Geysers. Additionally, the team studied networks with 25 and 100 stations using regularly and randomly spaced station distribution. Based on the hypocenter locations, the 3D velocity models, and the various network designs of seismic stations in the study area, the researchers numerically simulated seismic wave propagation and analyzed the resulting propagation paths through the 3D reservoir to estimate the resolution of the experimental design. In this investigation the total range in resolution of the seismic velocity estimates varied from 0-1, with 0 representing no resolution and 1 representing maximum resolution. The typical threshold for minimum resolution in tomographic studies is approximately 0.1, while values above 0.8 are rarely obtained in field experiments.

Figure 8 shows the two network geometries based on 100 stations as well as the outline of The Geysers geothermal reservoir (red polygon) superimposed on topographic maps. The black square indicates the study area of the current project. Green triangles denote the location of the seismic sensors that are part of the permanent seismic network, while the red dots in the study area represent two examples of the investigated network geometries. The results of the two network configurations with 10 x 10 regularly spaced stations and with 100 randomly spaced stations (Figure 8) is discussed following the figure.

Figure 8: Third-Generation Seismic Station Results

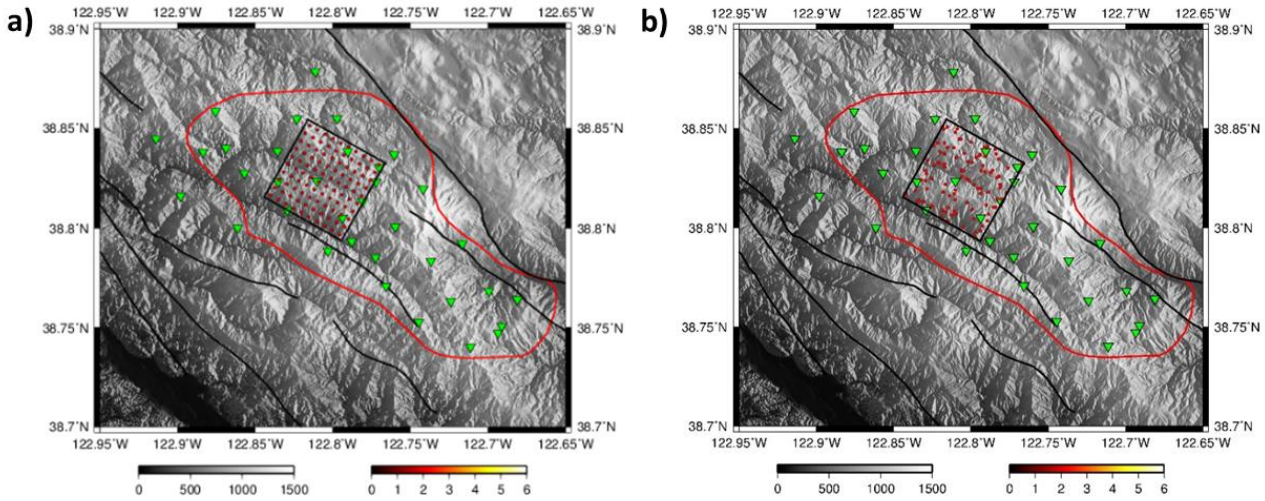

Topographic map displaying the outline of The Geysers steam field (red polygon), the LBNL permanent seismic network stations (green triangles), the 5 km by 5 km study area of the present project (black square), and (a) a regularly spaced 10 x 10 station network design (red dots), and (b) a network design with 100 randomly spaced stations (red dots). Black lines indicate known surface traces of faults.

Source: Lawrence Berkeley National Laboratory

Figure 9 shows the resolution analysis for the P-wave velocity estimates for the regularly spaced 10 by 10 station network and for the randomly spaced 100-station network. The plot shows a cubic display of the study area, with seismicity shown as colored dots. The majority of the events have a magnitude between 0.5 and 1.5. The measure of resolution is presented by the colored cubes denoted as derivative weight sum. For graphical reasons, a limited resolution range is plotted in Figure 9. The resolution is highest in the near subsurface below the stations and in the lower parts of the model where the earthquakes are clustered. This is cause by the higher number of seismic waves in these areas, which propagate from the earthquake hypocenters to the stations at the surface. Despite the stark differences in seismic station configuration, the resolution in the center of the reservoir is remarkably similar.

To better appraise the differences in performance between the two network configurations in Figure 9, the research team calculated differences in the resolution that are displayed in Figure 10. Figure 10a shows the areas where the regularly spaced network yields better resolution, while Figure 10b displays the areas where the randomly spaced network yields better resolution. For the randomly spaced network (Figure 10b), the resolution is higher in the shallow subsurface below the various cluster of stations. This is expected as the cluster of stations aggregates the seismic waves propagating towards them. Conversely, in regions where the randomly distributed station density is low, the resolution associated with the regularly spaced station configuration is higher (Figure 10a). The surprising lesson from this comparison is that the resolution in the center of the model is very similar in both cases. The conclusion is that given the same number of stations, the resolution in the reservoir is somewhat independent of the station design as long as the region of interest is deep enough below the surface.

Figure 9: P-Wave Resolution Estimate

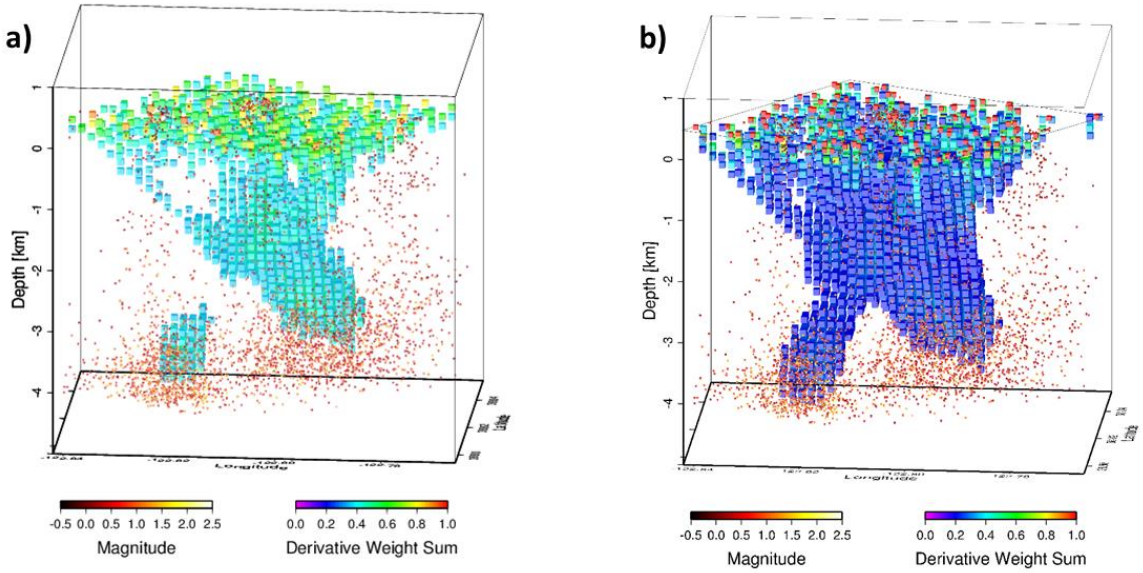

Resolution estimates of the P-wave seismic velocity estimates in the 5 km by 5 km study area at The Geysers. (a) Resolution for a 10 x 10 station regularly spaced network. Plotted range of resolution is 0.35 - 1.0 . (b) Resolution for a randomly spaced 100-station network. Plotted range of resolution is 0.20 - 1.0. The location of the random stations are denoted by the red cubes at the surface.

Source: Lawrence Berkeley National Laboratory

Figure 10: P-Wave Resolution Estimate Resolution Differences

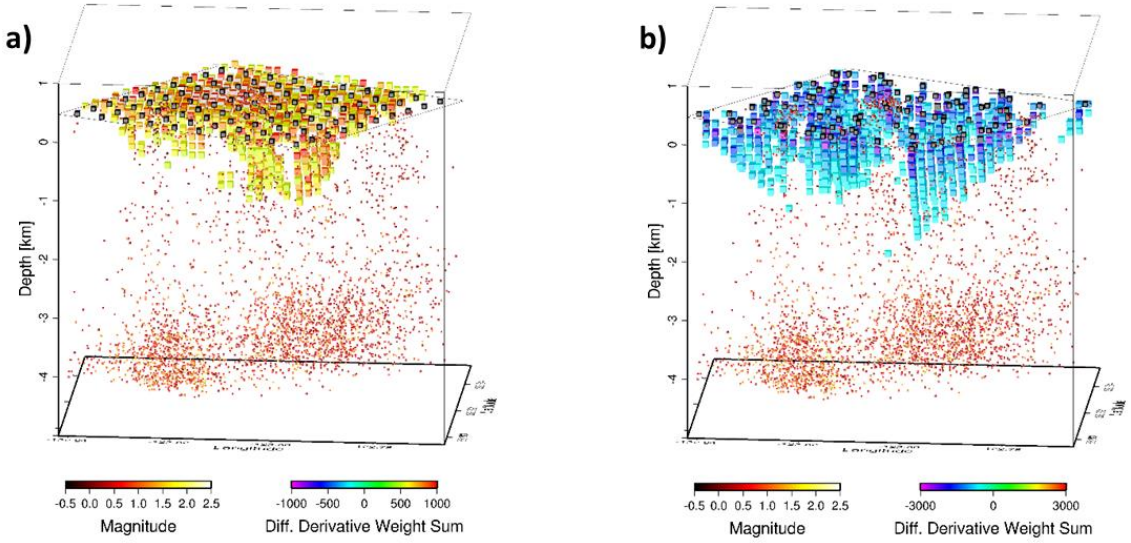

Difference in the resolution of P-wave velocity estimates between the regularly spaced station network and the randomly distributed station network in Figure 9a and 9b, respectively. The station locations are indicated by the black cubes at the surface. (a) Regions where the resolution estimates for the regularly distributed network are higher. (b) Regions where the resolution estimates for the randomly distributed network are higher.

Source: Lawrence Berkeley National Laboratory

The above result that a seismic network with regular-spaced or irregular-spaced stations will yield similar resolution is advantageous for the deployment at The Geysers because the extreme topography and vegetation coverage prevents a regular-spaced station deployment. Nevertheless, the goal was to deploy stations as regularly spaced as possible and in quantity as close as possible to the maximum number of 100 stations. The deployment was done over three weeks in April and May 2018, when 91 stations were sited. Of the 91 stations, five stations were co-located with stations of the permanent seismic network. These stations include BGCLV, BGBUC, BGNEG, BGSB4, and BGSQK. Nine stations could not be deployed due to excessive vegetation coverage or inaccessibility of the originally planned locations. Figure 11 presents the final locations of the network stations. The figure shows that despite the challenging environment, the network stations reveal a high degree of regular spacing at approximately 500 m offset.

Figure 11: Final High-Density Seismic Network

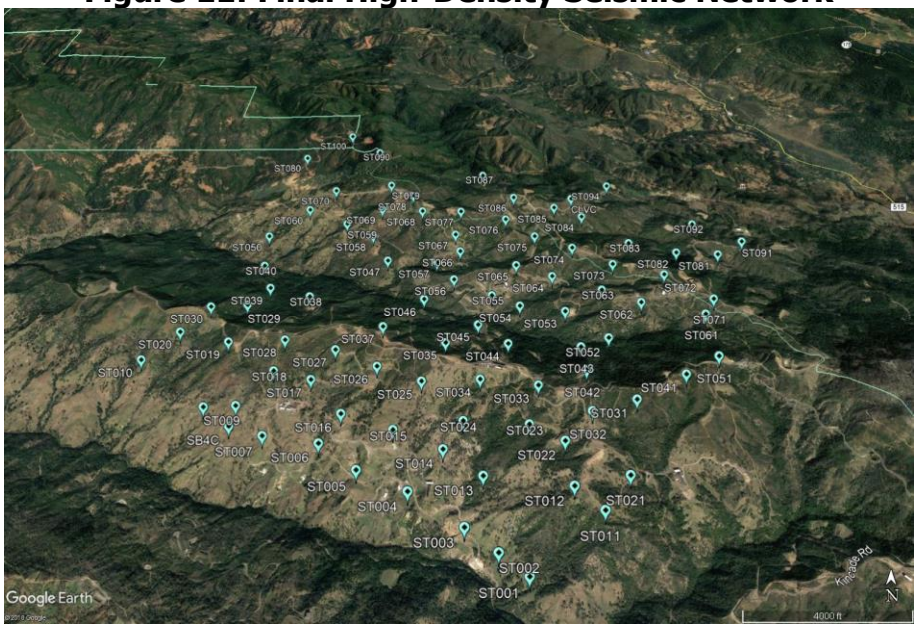

Final seismic network configuration with 91 seismic station distributed over the 5x5 km study area at The Geysers geothermal reservoir.

Source: Lawrence Berkeley National Laboratory

Development of Seismic Data Processing Software

JDS performed seismic data processing based on the REMAS and PhaseNet (Zhu and Berosa, 2019) software packages, which perform fast, automated processing of micro-earthquake data from dense networks. This software provides complete data processing including phase detection, event association and location, estimation of phase travel time, pulse width, event moment magnitude, seismic moment, generation of waveforms, and storage of parameters in database. Figure 12 summarizes the workflow of data processing, which consisted of various processes executed sequentially from the raw data to the final seismic data products that are subsequently used to analyze micro-seismic event locations and to image seismic velocities and attenuation in the reservoir. Specifically, the workflow commenced with reading and copying the raw data from the secure digital (SD) cards to a computer hard drive, followed by a search for the quietest 15 stations to run an event detector on the continuous data. The

event detector returned seismic phases that rise above the noise level for a predefined threshold on each of the 15 stations. The researchers subsequently analyzed these phase detections for possible association with a seismic event if they were observed on a minimum of 10 stations. Once an event was detected, appropriate time windows were calculated for each station and the associated waveforms were extracted from the continuous recordings. This was followed by the estimation of P-wave phase arrivals for each station. The determination of S-wave phase arrival times was achieved by rotating the horizontal components of each station to maximize S-wave amplitudes for easier phase arrival estimation. The research team used the combination of P- and S-wave arrivals to determine the preliminary hypocenter of the event. The arrival times of P- and S-wave phases were subsequently used to determine P- and S-wave pulse widths and first motion polarity. All parameters were loaded into a database and input files for tomographic imaging with the programs SimulCR and tomoFDD were generated. In addition to these input files, waveform cross correlations between events were computed for differential travel time analysis by tomoFDD. Using this processing scheme, the research team detected and analyzed more than 17,000 events in the study area.

Figure 12: Schematic Workflow of the Seismic Data Processing

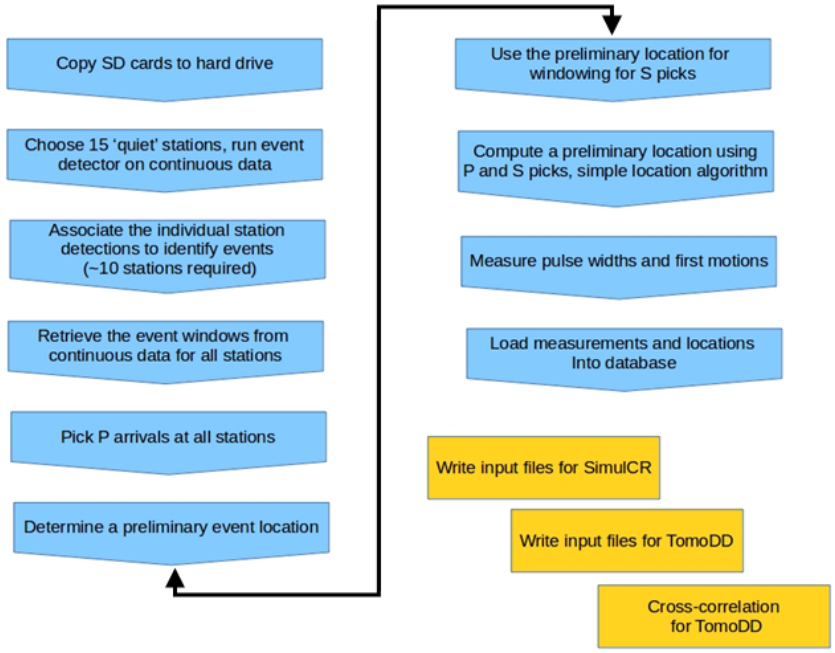

Schematic workflow of seismic data processing.

Source: Lawrence Berkeley National Laboratory

Field Demonstration of Seismic Network

The researchers evaluated the performance of the low-cost seismic stations (referred to as "CEC network" or "CEC stations") compared to the permanent network stations shown in Figure 8 (in the following referred to as BG network or BG stations) using data recorded from May 2018 to October 2018. During this period, the CEC network recorded 6,218 events in the 5x5 km study area while the BG-network recorded about 2,000 earthquakes. The reason for this discrepancy is the high number and greater proximity of CEC-stations above the 5x5 km study area, while the 34-station BG-network is spread throughout the extent of The Geysers

reservoir (~ 20x10 km area). The proximity of the CEC-stations to the earthquakes in the study area enables the network to capture events with lower magnitudes, while the waves of these smaller events are attenuated during their propagation to the BG-stations at longer distances and thus not detected. In contrast, the amplitudes of waves associated with higher magnitudes saturate the near CEC-stations, so that phase arrival times and hypocenters cannot be determined, while the BG-stations at longer distances are able to record and locate the higher magnitude events. This is also emphasized in Figure 13, which shows a histogram of the magnitude distribution for both networks. The histogram for the CEC-network in Figure 13a shows that the maximum number of events were observed for a magnitude of moment magnitude (Mw)=0.4 level, while the magnitude range reaches from to Mw=-0.4-2.8. The histogram of the BG-network (Figure 13b) reveals a different distribution with the maximum number of events observed for a magnitude of Mw=0.9 and a total magnitude range from Mw=0.0-3.8.

Figure 13: Schematic Workflow of the Seismic Data

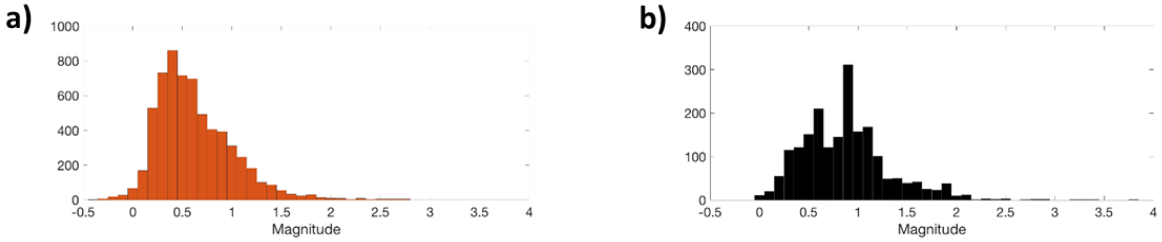

Histogram of moment magnitude distribution for the CEC-network (a) and the LBNL BG-network (b).

Source: Lawrence Berkeley National Laboratory

The researchers evaluated data quality with seismic waveforms recorded by those CEC stations that were co-located with permanent stations of the LBNL seismic network. The following example is provided for stations CGSB4 (CEC station) and BGSB4 (permanent LBNL network station), which are co-located along the south-western margin of the 5x5 km study area. The team evaluated data in the time and spectral domain, after waveforms were corrected by the instrument response of the two seismic sensors, and selected an event with moment magnitudes of 1.0 for comparison. The waveforms recorded by the two co-located sensors are superimposed in Figure 14. The figure presents the waveforms of the permanent LBNL station in black and those of the CEC station of the current project in red. It can be seen that the waveforms match quite well, not only for the P- and S-wave phases but also for the noise and scattered phases throughout the traces.

Figure 14: Comparison of Waveforms Recorded by CEC and Permanent Station

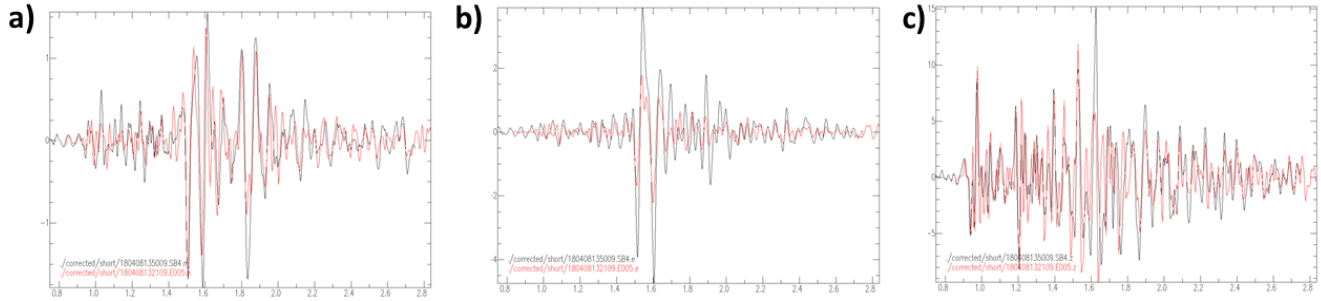

Seismic waveforms recorded by the permanent LBNL stations BGSB4 (black) and by the CEC stations CGSB4 of the current project (red) for an earthquake with moment magnitude Mw=1.0. (a) North component. (b) East component. (c) Vertical component.

Source: Lawrence Berkeley National Laboratory

The amplitude spectra of the Mw=1.0 event are presented in Figure 15. The spectra include all three components for the permanent station BGSB4 (black lines) and for the CEC station CGSB4 (red lines). The spectra reveal the same shape over the frequency range from 0.01 to 100 Hz, with similar amplitudes from the noise level at 1 Hz to the maxima at 10 Hz and to the fall-off from 10 to 100 Hz. However, between 1 and 10 Hz, station CGSB4 reveals slightly lower amplitudes than station BGSB4. This slight discrepancy is inconsequential, however, since the data in this frequency range represent ambient noise, while the seismic data are observed above 10 Hz.

Figure 15: Comparison of Spectra Recorded by CEC and Permanent Station

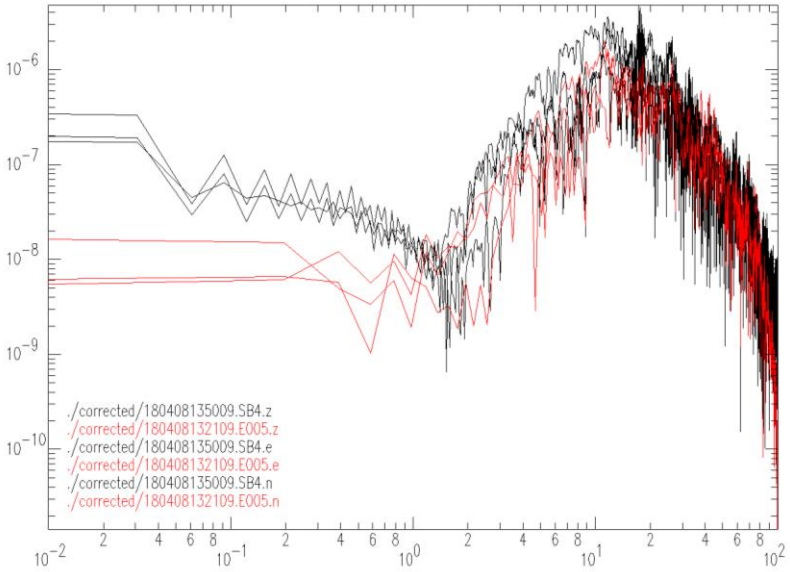

Amplitude spectra of the x-, y- and z-component recorded by the LBNL station BGSB4 (black) and by the CEC stations CGSB4 (red) for the Mw=1.0 event.

Source: Lawrence Berkeley National Laboratory

Overall, the co-located stations show good agreement in the recorded waveforms and the spectral content of the seismic waves. This result gave confidence that the seismic data recorded by the CEC network is representative of the seismic wavefield generated by

earthquakes in the study area and that they can be used for seismic imaging of reservoir properties.

Optimization of Code Base for Seismic Imaging

The research team used two 3D inversion codes primarily to generate images of the reservoirs P- and S-wave velocities and P- and S-wave attenuation distribution. The codes, SimulCR and tomoFDD are conceptually similar and originate from the similar family of codes: SimulPS (Thurber, 1983; Eberhart-Phillips, 1986) and hypoDD (Waldhauser and Ellsworth, 2000). SimulCR and tomoFDD simultaneously invert for the 3D velocity and attenuation structure as well as for the earthquake hypocenter locations. Both codes solve the hypocenter location problem in an absolute and a relative way. The relative location part is performed using the principle of differential travel times that eliminate most of the effects along the raypaths from two neighboring events to a common recording station. The principles of the two codes are briefly described below.

Inversion Code tomoFDD

The inversion code tomoFDD is a combination of hypoDD (Waldhauser and Ellsworth, 2000) and tomoDD (Zhang and Thurber, 2003). tomoFDD also uses absolute and differential P- and S-wave arrival times in a joint solution for event locations and 3D P- and S-wave velocity structure. However, tomoFDD does not solve for attenuation. Many fields of science use the concept of double-difference, in which the elimination of common path effects suppresses the impact of the Earth property model uncertainties. The concept applies when the distance between neighboring earthquakes is small relative to the length of propagation paths to a common recording station. Calculating the differences in travel times thus eliminates path effects from the earthquakes to the station at the surface. Because relative times are more accurate than absolute times, this method recovers more accurate event locations and velocity structure near the source region than standard tomography and sharpens the velocity image in the source region due to the combination of the higher accuracy differential time data and the concentration of corresponding model derivatives in the source region. Rather than assigning maximum interevent distances and searching the event catalog for pairs that satisfy the double difference criterium, the research team employed waveform cross correlation for all events recorded at a common station and setting the minimum correlation coefficient to 0.8 to assure that the events are practically co-located and share a common ray path. tomoFDD uses a finite difference eikonal solver (Podvin and Lecomte, 1991) to compute synthetic travel times based on an a priori 3D velocity model and also employs least-squares to iteratively minimize the misfit between the observed and computed travel times to obtain a smooth 3D velocity model during the inversion.

tomoFDD was upgraded to Fortran90 in 2012 to take advantage of dynamic memory allocation, which enables the code to allocate and deallocate memory for any field or array as they are accessed during computation. The advantage is that larger data arrays can be assigned during the inversion because most are not accessed simultaneously. In contrast, earlier versions of Fortran, such as Fortran77, assign fixed memory allocations for each field and array during the compilation of the source code even though those fields and arrays are accessed at different time during the computation. Considering a given amount of computer memory, this fixed memory allocation severely limits the field and array sizes available during

computation. The conversion of tomoFDD to Fortran90 was undertaken for a past project to conduct joint inversions of earthquake hypocenter locations and 3D velocity structure at The Geysers geothermal reservoir, where seismic travel time data from more than 30,000 earthquakes were used in the inversions (Gritto et al., 2013a). The conversion to Fortran90 and the use of the fast finite difference eikonal solver (Podvin and Lecomte, 1991) make tomoFDD well suited for the current project where the combination of a high number of stations, a high volume of recorded earthquake data and a high number of inversion nodes pose great demands on computer memory and CPU speed. The inversions with tomoFDD for the current project will run with a node spacing of 150 m, which provides sufficient resolution for the goals of the current project.

Inversion Code SimulCR

The inversion code SimulCR uses absolute P- and S-wave travel times to invert for absolute earthquake hypocenter locations and the 3D P- and S-wave velocity structure in the subsurface. The code also uses the pulse width of the recoded P- and S-waves to invert for the attenuation structure Q_P and Q_S. In addition to the absolute travel times, SimulPS uses relative travel times for events that share the "same raypath" to a common recording station. The purpose is to eliminate path effects along the common path from the events to the recording station, which improved travel time accuracy. Applying the common ray principle to the relative travel times yields improved hypocenter locations. The advantages include accurate absolute hypocenter locations and improved relative locations, which help to delineate fracture zones or earthquake clusters and refine the velocity and attenuation models around these earthquakes. SimulPS uses ray bending to compute synthetic travel times based on an a priori 3D velocity model and employs least-squares to iteratively minimize the misfit between the observed and computed travel times to obtain a smooth 3D velocity model during the inversion.

During code optimization the researchers investigated whether multithreading could be added to SimulCR. Multithreading splits loop iterations among the available computer cores and executes them in parallel. To take full advantage of multithreading, slow loops need to be configured such that each iteration can run independently of the other iterations. Threads that are not independent execute slower and are more error prone, so multithreading has the potential to decrease the run-time. However, because SimulCR is large, complex, and not designed to have multithreaded loops, adding multithreading would have required extensive restructuring of the source code, which was beyond the scope of this project. Considering the complications to implementing multithreading, combined with the poor decrease in run-time, led to abandoning implementing multithreading to SimulCR.

The original goal was to run SimulCR with a node spacing of 125 m, which required a conversion from Fortran77 to Fortran90 because common blocks needed to be changed to modules, a feature added in Fortran90. Modules allow the use of 16-byte parameters. The 125 m node spacing required one of the parameters to be converted to 16 bytes, which increased its memory requirements exponentially and requires execution on a computer with sufficient memory. However, testing revealed the CPU times for inversions with 125 m node spacing were impractical for the current project. As a consequence, researchers selected a node spacing of 250 m for the inversions with SimulCR.

Rock Physics Transformation of Seismic Images

The goals of this task included the development of correlations between seismic properties and rock and fluid properties, realizing that this transformation is not unique. To be useful to Calpine Corp. it was important to develop simple transformation approaches that have clearly defined bounds of applicability and a solid physical basis. The analyses included a data-driven approach in which the research team examined correlations between well data and seismic properties and determined whether relationships could be established for steam/water saturation regimes. In constructing these relationships, Calpine can use the results of this study to better target future well placements.

Past studies have shown that seismic P-wave velocity (V_P) and S-wave velocity (V_S) can be used to differentiate different classes of rock, while Vp/Vs ratio can be used to interpret the physical properties of the fractures that naturally occur in the different rock types. Numerous studies have shown that high Vp/Vs is often associated with fluid-filled fractured rock, while low Vp/Vs is related to dry and gas-filled rocks. At The Geysers, high Vp/Vs relates to water-saturated zones due to fluid injection, while low Vp/Vs relates to regions where steam is predominantly present due to the continuous boiling of interstitial water to steam, particularly in the high-temperature reservoir of the NW Geysers. The relationship between Vp/Vs ratio and water content at The Geysers geothermal reservoir was documented by, for example, Gritto and Jarpe (2014).

In this project, the research team used the relationships between seismic velocities and water and steam saturations of reservoir rock to delineate reservoir heterogeneity, subsurface fluid flow, flow barriers, and target zones for future steam production. This team accomplished this by combining the 3D seismic imaging results with The Geysers 3D geothermal reservoir model using the SKUA/GOCAD code family. The Geysers comprehensive 3D reservoir model, developed by Hartline et al. (2015; 2016; 2019), includes structural controls such as fault and fracture surfaces, water injection and steam production volumes, fracture densities encountered in boreholes, and many other features that are important for the interpretation of the seismic imaging results as well as for the elastic moduli, which were derived from the seismic velocities. The joint interpretation of the 3D velocity data and elastic moduli between the research team and Calpine staff was an integral part of the current project. This step improved Calpine's confidence in the tomographic inversion results, which will support their drilling program to minimize drilling of unsuccessful wells.

CHAPTER 3:
Project Results

Seismic Tomographic Imaging

During this project, researchers processed seismic travel time and pulse width data for the data recorded by the 91-stations high-density network presented in this chapter. The processing resulted in detection and location of more than 17,000 events with more than 634,000 P-wave and more than 595,000 S-wave phase arrivals, while the number of pulse width measurements equals the number of phase picks for each wave. The research team subsequently used the processed data during seismic tomographic imaging to locate earthquakes and obtain the 3D P- and S-wave velocity and attenuation structure. In addition to 3D images of the velocities and attenuation, the team compiled refined catalogs of earthquake hypocenter locations, origin times, and seismic moments. The following examples present the results.

Figure 16a presents a histogram with the distribution of moment magnitudes for the 17,000 analyzed events. While the histogram shows a magnitude range from 0 ≤ Mw ≤ 3, the maximum number of events is observed at Mw = 0.4. Figure 16b shows the relocated earthquakes resulting from the tomographic inversion of the seismic data, which shows the 5 x 5 km study area indicated by the green square, the 91-station seismic network represented by the cyan-colored triangles, and the 17,000 earthquakes by the circles color-coded for hypocentral depth. The events cover a region beyond the study area and range from 0 km to 6 km depth. While there exists a mix of shallow and deep events in the reservoir below the study area, the seismicity reveals a general trend of shallower events in the south-east and deeper events in the north-west. This trend is a manifestation of the extent of the geothermal reservoir to greater depth towards the north-west.

Figure 16: Histogram of Magnitude and Hypocentral Depth of Analyzed Events

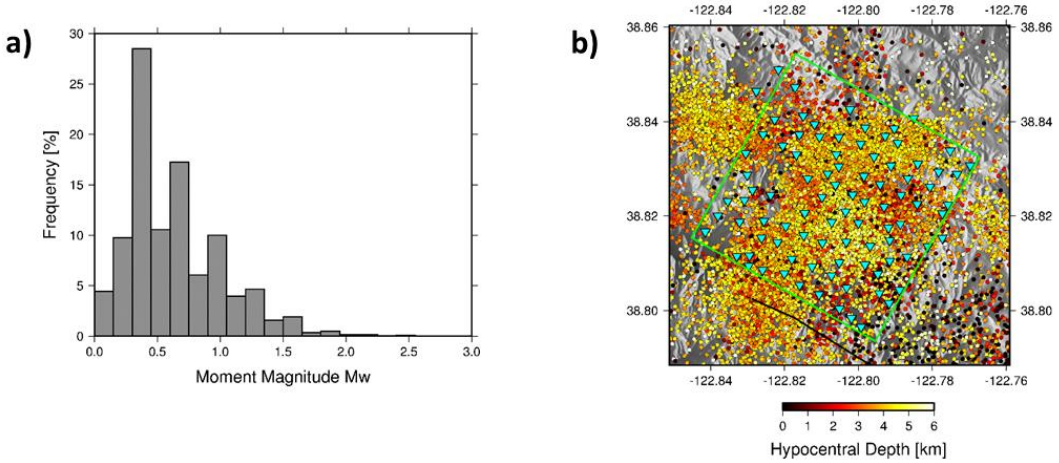

(a) Histogram with moment magnitude (Mw) distribution for the set of 17,000 analyzed events. (b) Map view of relocated seismicity resulting from seismic tomographic inversion of the 17,000 events. The seismicity is color coded for hypocentral depth.

Source: Lawrence Berkeley National Laboratory

Figure 17 presents the seismic P-wave velocity estimates obtained from the travel time inversion. The velocities are only plotted in regions that have sufficient resolution. However, due to the high density of seismic events (Figure 16b), the resolution is sufficient throughout most of the study region. Figure 17a shows a map of the felsite interface with the locations of the study area and of the velocity profiles. The Felsite, a granitic pluton that intrudes the bottom of the reservoir, is considered the heat source of the geothermal resource. In all three vertical profiles (Figure 17b-c), the shallow parts of the reservoir exhibit intermediate P-wave velocities between Vp = 4.0 – 5.0 km/s, with lower values in the north-west and higher values in the south-east of the study area. This layer represents the Greenstone caprock, which is deepening towards the northwest. The velocities are increasing to Vp = 5.5 km/s at the top of the reservoir, where Graywacke represents the main reservoir rock. Gradual deepening into the reservoir is accompanied by increasing velocity values from Vp = 5.5 – 6.0 km/s, which represents Hornfels, a metamorphosed phase of Graywacke. The Felsite is finally encountered in the lower part of the reservoir with velocity values ≥ Vp = 6.0 km/s. The velocity profiles indicate nicely how the P-wave velocity can be used to image and delineate the different rock types in the reservoir.

Figure 17: Seismic P-Wave Velocity Profiles

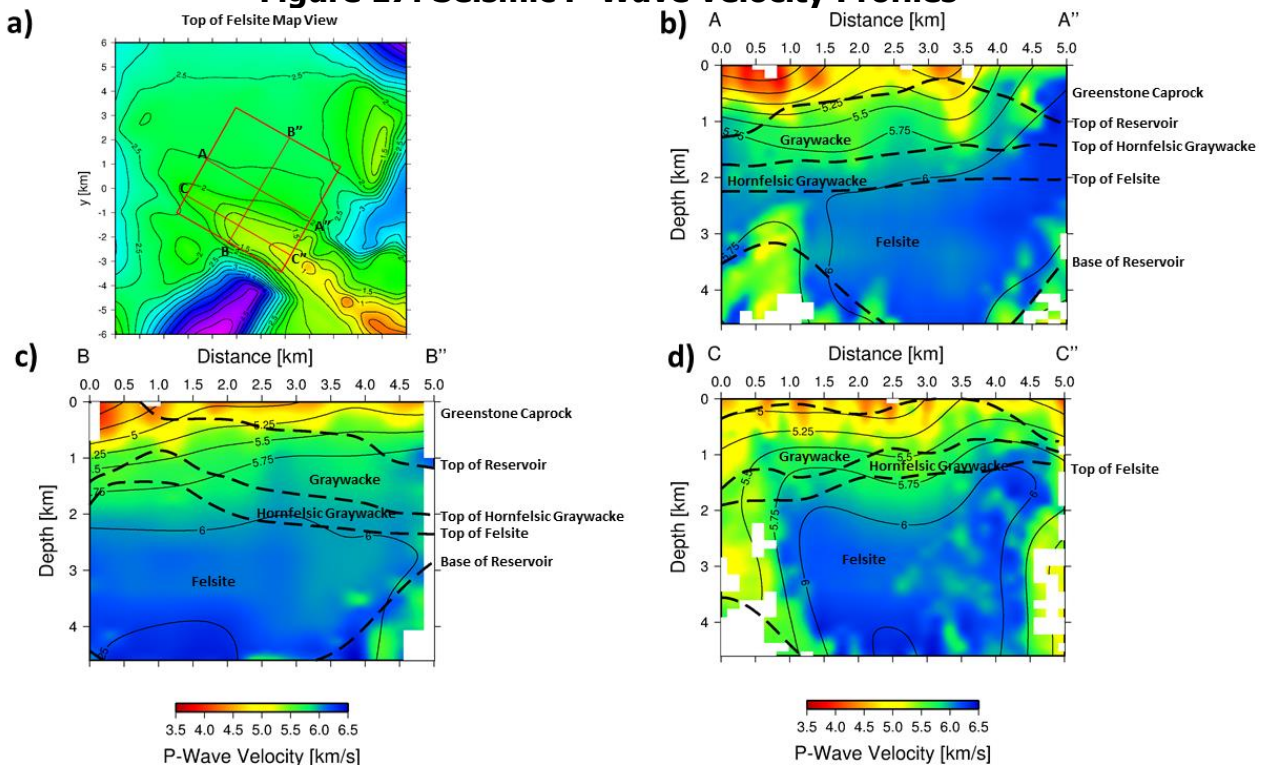

(a) Map view of the top of Felsite interface with locations of the study area and of the vertical velocity profiles. (b) Vertical cross section through the P-wave velocity estimates along profile A-A". (c) Vertical cross section through the P-wave velocity estimates along profile B-B". (d) Vertical cross section through the P-wave velocity estimates along profile C-C". The dashed lines are geological interfaces from the 3D geothermal reservoir model, derived from borehole observations.

Source: Lawrence Berkeley National Laboratory

Figure 18a,b display the S-wave velocities, similar to the seismic P-wave velocities. Figure 17a presents the vertical cross sections for the profiles A-A' and B-B". The S-wave velocities also show a gradual increase from Vs = 2.5 km/s for the caprock, to Vs = 3.0 km/s for the

Graywacke, to Vs = 3.3 – 3.7 km/s for the Hornfels, and to Vs = 4.0 km/s for the Felsite, and can also be used to delineate the geothermal rocks in the reservoir.

The Vp/Vs-ratio is often used to interpret physical parameters in the subsurface. High Vp/Vs-ratio is typically associated with fluid filled fractured rock (Moos and Zoback, 1983, Gritto et al., 2004), while low Vp/Vs is related to dry and gas filled rocks. At The Geysers, high Vp/Vs relates to water saturated zones due to fluid injection and low Vp/Vs to regions where steam is predominantly present due to flashing of water to steam (Gritto et al., 2013a, Gritto and Jarpe, 2014). Correlating Vp/Vs anomalies to observed seismicity allows researchers to draw conclusions about the state of the reservoir, so the current project investigated the Vp/Vs-ratio.

Figure 18c,d shows the estimates for the Vp/Vs-ratio below the study area for the same selection of horizontal depth slices as before. Because Vp/Vs-ratio is computed by taking the ratio of the P-wave and S-wave velocity estimates, the resolution for Vp/Vs-ratio is taken from the S-wave resolution as it is lower than the P-wave resolution. In the shallow parts of the reservoir the Vp/Vs-ratio is heterogeneous with low values (1.4) in the north-west and high values (2.0) in the northeast. These may indicate steam and water saturated areas, respectively, and may relate to injection and production activities. With increasing depth, the Vp/Vs-ratio drops to values around Vp/Vs = 1.55 – 1.65 as can be expected for a steam dominated reservoir such as The Geysers.

Figure 18: Seismic S-Wave and Vp/Vs Velocity Profiles

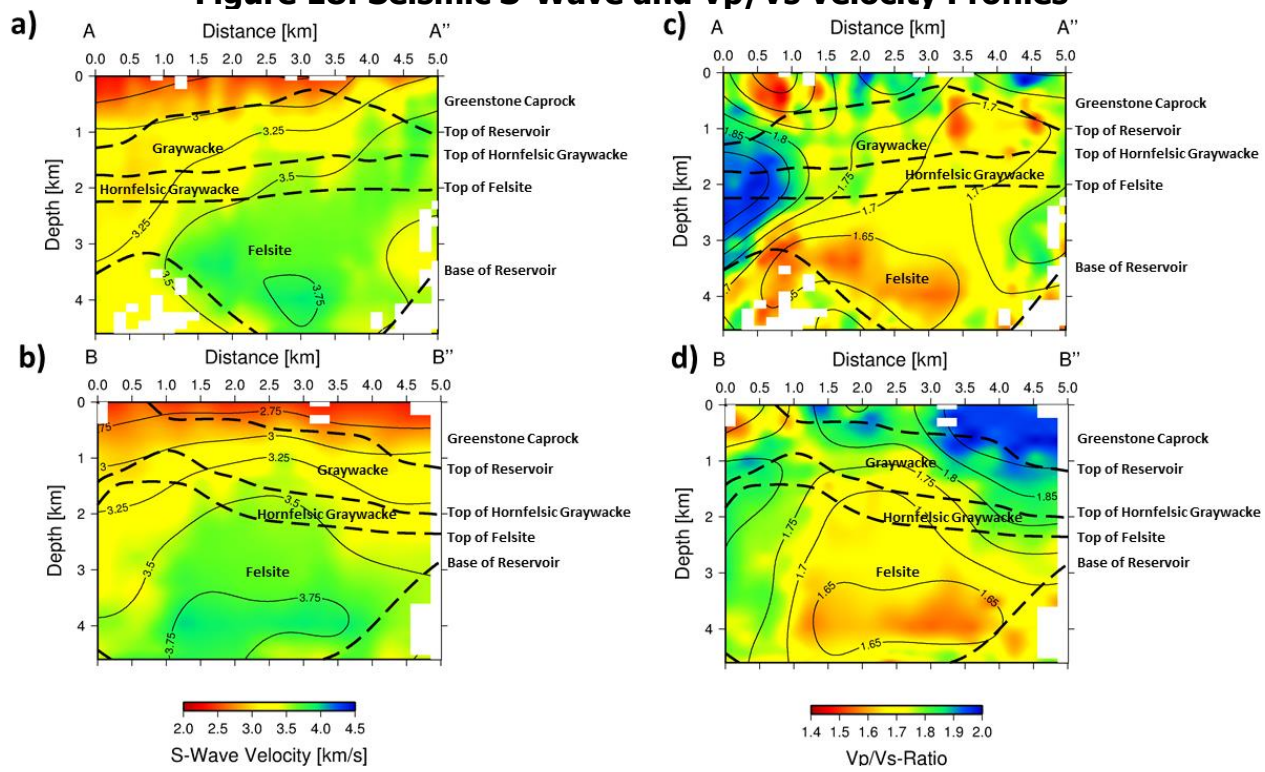

S-wave velocity and Vp/Vs-ratio cross sections along profiles shown in Figure 17a. (a) Vertical S-wave velocity cross section along profile A-A". (b) Vertical S-wave velocity cross section along profile B-B". (c) Vertical Vp/Vs-ratio cross section along profile A-A". (d) Vertical Vp/Vs-ratio cross section along profile B-B".

Source: Lawrence Berkeley National Laboratory

The following section examines the correlation between seismic attributes and reservoir injection and production more closely.

Correlations of Seismic Attributes to Reservoir Operations

In addition to structural controls of the reservoirs, such as rock geological interfaces faults and fractures, the 3D geothermal reservoir model also includes the trajectories of water injection and steam production wells. The first appraisal of the tomographic images included the spatial correlation of P-and S-wave velocities and Vp/Vs ratio to water injection and steam production wells. Figure 19 provides an example of the 3D P- wave and S-wave velocity models and water injection and steam production. The size and location of the blue and red spheres represent the volume and the depth of water injection and steam production, respectively. Figure 19a,b displays the P-wave velocity model, which indicates a velocity gradient with lower velocities (orange) in the near surface, intermediate velocities (yellow/cyan) below the surface layer, and high velocities (blue) in the deeper region of the reservoir, which constitutes a manifestation of the major geological formations in the reservoir. A closer inspection of the velocity estimates in the vicinity of the steam entries (red spheres) reveals a "pull-down" of the lower velocities (orange) to intermediate reservoir depth. These features indicate the presence of steam saturated zones surrounding the production wells in this part of the reservoir, as will be shown below. Conversely, the velocity estimates in the vicinity of the water injection (blue spheres) reveal a "pull-up" of the higher velocities (blue) to intermediate reservoir depth. The water injection wells have open-hole sections along the borehole, which allows water to flow into the reservoir rock. These velocity anomalies could indicate an increase in water saturation in the vicinity and below the water injection wells. In contrast, Figure 19c,d, which display the S-wave velocity model, do not show a strong correlation with the water injection and steam production. This can be expected considering the properties of shear waves, which are much less sensitive to fluid saturation in the subsurface. The example shows that the 3D velocity model can be used for geological and structural interpretation as well as for delineation of the heterogeneity in water and steam saturation.

Earlier it was shown that the Vp/Vs ratio reveals a higher degree of heterogeneity within the reservoir than the P- and S-wave velocities because Vp/Vs is more affected by water injection and steam production operations (Gritto et al., 2020). Figure 20 shows this concept in a map view of the Vp/Vs ratio at 700 m depth (Figure 20a) and related fence diagrams with views from south-east (Figure 20b) and from south-west (Figure 20c). For the purpose of improved visualization, the researchers selected a group of injection wells in the western part of the study area for correlation to the Vp/Vs ratio. Steam entries in Figure 20 are represented by discs that transect the well trajectory orthogonally at the depth of the steam encounter. The size of the disc is proportional to the steam pressure encountered at that depth during drilling of the wells. The Vp/Vs ratio in Figure 20a shows a low anomaly (Vp/Vs ~ 1.5) in the vicinity of the steam production well, which is indicated by the round disc. The Vp/Vs anomaly appears extensive at this depth level extending outward from the production well. The fence diagrams in Figure 20b,c provide additional perspectives where the group of selected steam production wells are indicated by the trajectories through the 3D model. The largest steam entry disc is partially obscured by the vertical sections, as they are centered on the location of the steam entry in the well. Nevertheless, the figure shows that the steam entry correlates very well with the low Vp/Vs anomaly surrounding this borehole. Figure 20c also reveals that

the group of wells in the southwestern-most corner of the study area also displays steam entries that correlate well with low Vp/Vs anomalies. However, the steam entries and Vp/Vs anomalies are smaller than in the previous example. These results show the potential use of the Vp/Vs response to better understand the directionality of the of water and steam movement within the reservoir.

Figure 19: Spatial Correlation of Seismic Velocities and Injection/Production Wells

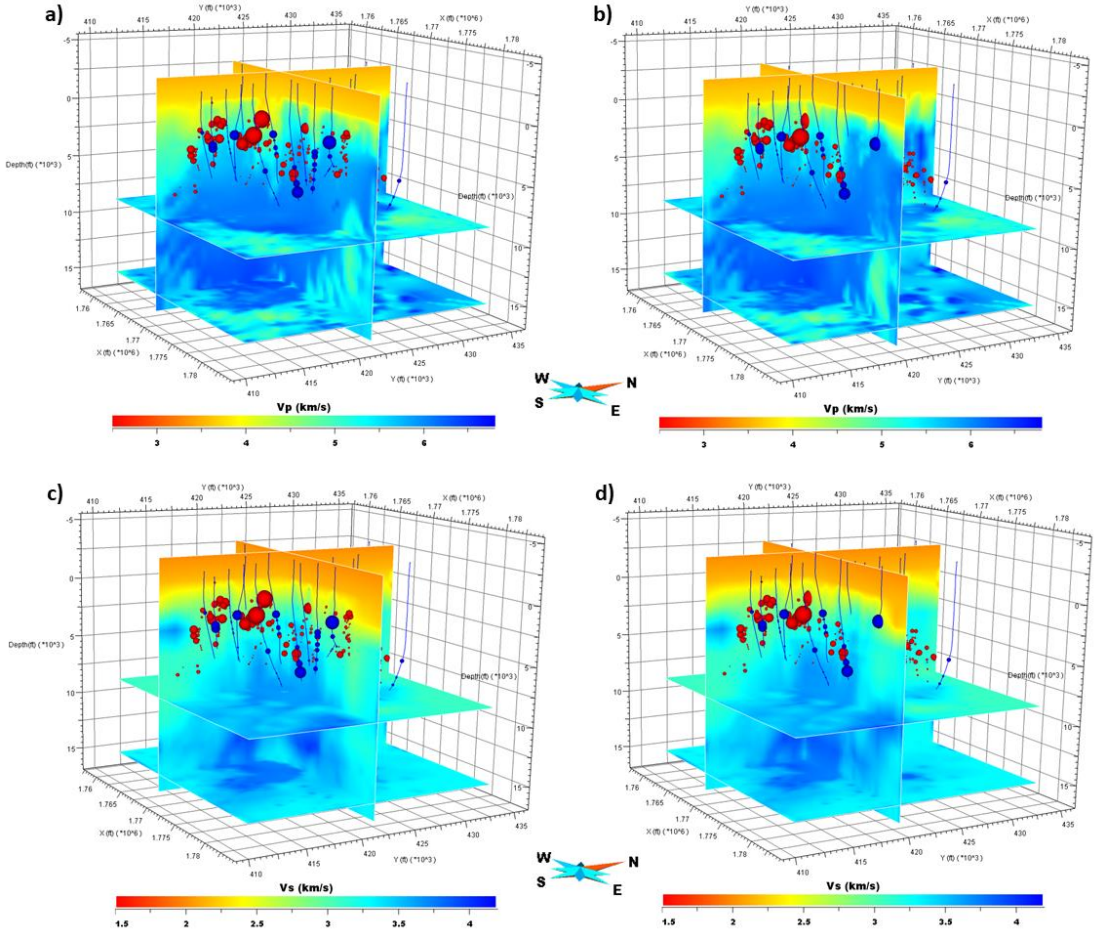

Fence diagram through the 3D P-wave velocity model with water injection and steam production superimposed, respectively, by the blue and red spheres. (a) and (b) represent different cross sections through the 3D P-wave velocity model. (c) and (d) represent different cross sections through the 3D S-wave velocity model.

Source: Lawrence Berkeley National Laboratory

Figure 20: Spatial Correlation of Vp/Vs-Ratio and Production Wells

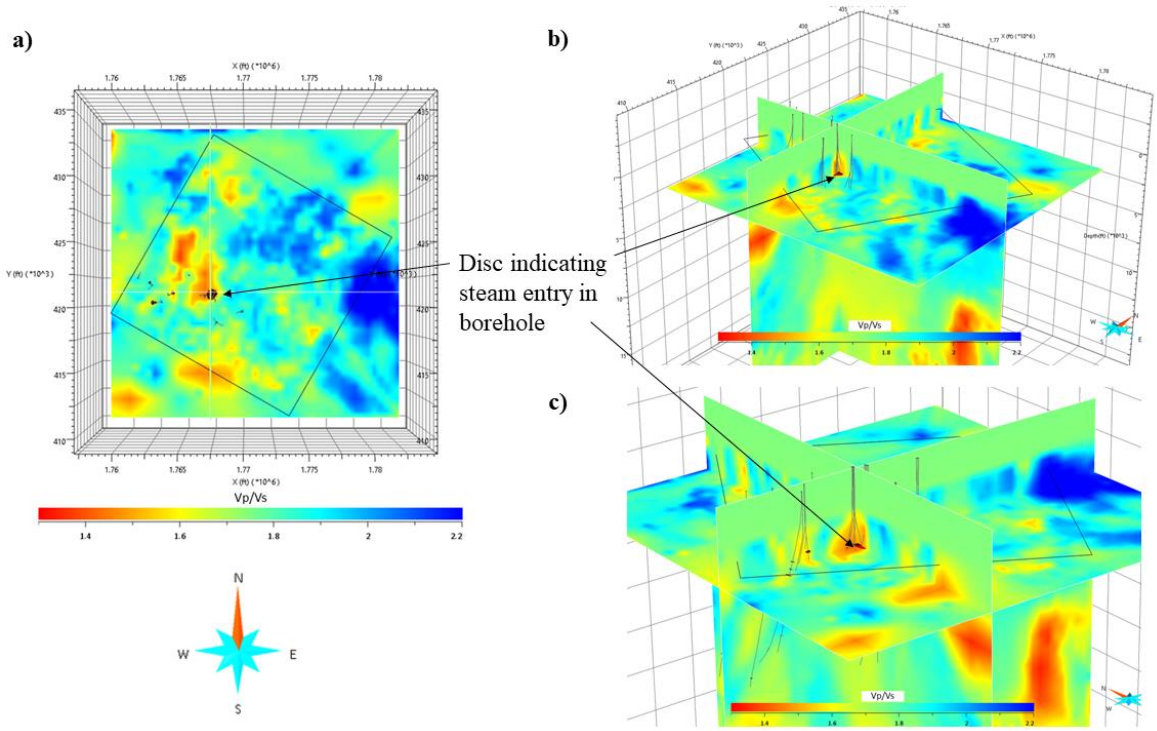

(a) Map view of the Vp/Vs ratio at 700 m depth. The back square denotes the 5x5 km study area, while the short black lines in the western part of the image are projections of the well trajectories of a group of injection wells. (b) Fence diagram through the Vp/Vs model with a group of steam production wells superimposed. The small red symbols cutting orthogonally through the well trajectories represent the volume of steam encountered in the well. View from south-east. (c) Fence diagram through the Vp/Vs model with a group of steam production wells superimposed. The small red symbols cutting orthogonally through the well trajectories represent the volume of steam encountered in the well. View from south-west.

Source: Lawrence Berkeley National Laboratory

Figure 21 shows the spatial correlation of Vp/Vs ratio to regions with increased water injection. The fence diagram in the figure reveals the Vp/Vs ratio and is aligned on a red sphere representing steam production in the center (red arrow), while crossing next to the large blue water injections sphere near the top of the east-west cross section at shallow depth in the foreground (blue arrow). Again, the size of the spheres is proportional to steam production and water injection volumes during the 2018-2019 study period at that depth in the wells. The partially visible red sphere in the center of the cross sections is surrounded by low Vp/Vs values (red-orange anomaly). The low Vp/Vs anomaly indicates the presence of steam in the imaged rock mass, which is corroborated by the high volume of steam production observed at that depth in the production well. Conversely, the large blue sphere in the top foreground in Figure 21 is located adjacent to very high Vp/Vs anomalies in the shallow eastern region of the study area that were already visible in the fence diagrams in Figure 20. The large size of the sphere indicates high volumes of injected water, which likely saturated the reservoir adjacent to the water entry. The water-saturated reservoir rock generated high Vp/Vs ratios in the tomographic images, confirming the correlation between high Vp/Vs and high-water saturation. The examples in Figure 19, Figure 20, and Figure 21 show promise in using seismic properties to delineate liquid types (water/steam) in the reservoir including the directionality of water and steam movement.

Figure 21: Spatial Correlation of Vp/Vs-Ratio and Injection Wells

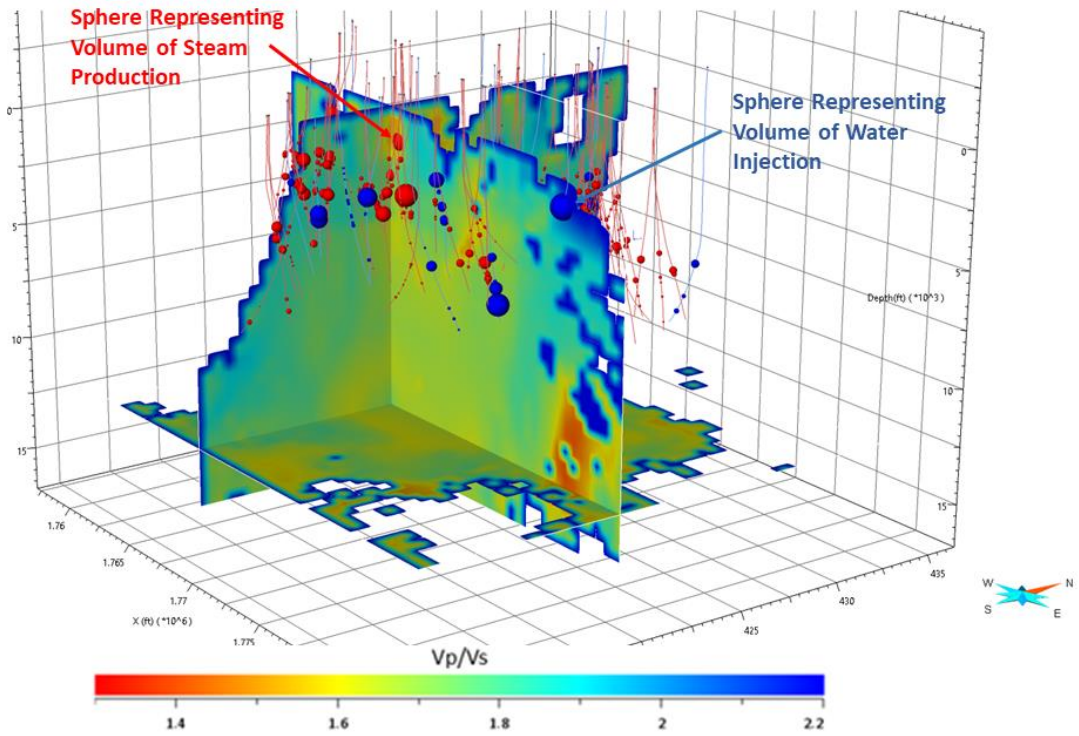

Fence diagram through the Vp/Vs model with steam production wells (red trajectories) and water injection wells (blue trajectories) superimposed. The red and blue spheres represent, respectively, the amount of steam produced, and the amount of water injected. The fence diagram is aligned on one steam production sphere in the center and crosses near the large blue water injections sphere near the top of the east-west cross section at shallow depth in the foreground. View from south-west.

Source: Lawrence Berkeley National Laboratory

Correlation of Seismic Attributes and Elastic Moduli to Structural Reservoir Features

Researchers conducted the correlation analysis of the velocities and elastic moduli to structural features in the reservoir in close collaboration with Calpine Corp. The research team shared the 3D velocity and elastic moduli models of the reservoir with Calpine and incorporated them into Calpine's comprehensive 3D reservoir model via the SKUA/GOCAD software package. The Geysers comprehensive 3D reservoir model, developed by Hartline et al. (2015; 2016; 2019), includes structural controls such as fault and fracture surfaces (Figure 3 and Figure 4), water injection and steam production volumes, fracture densities encountered in boreholes, and many other features that are important for the interpretation of the seismic imaging results as well as for the elastic moduli, which the research team derived from the seismic velocities as presented in Appendix A. The joint interpretation of the 3D velocity data and elastic moduli between the research team and Calpine staff was an integral part of the current project. This step improved Calpine's confidence in the tomographic inversion results, which will support its drilling program to minimize drilling of unsuccessful wells.

The following section provides examples of correlations between seismic velocities, elastic properties, and structural features in the 5x5 km study area. Figure 22 depicts the Vp/Vs ratio (colored dots) representing a flow path of water from the location of water injection well Prati 9 to the Big Sulphur Creek (SCF) fault. The location of Prati 9 is represented by the cyan-colored disc below the northwestern boundary of the study area, while the location of the SCF is shown schematically by the dashed line striking parallel along the southwestern boundary of the study area. The SCF is impervious to fluids and constitutes a southwestern barrier to the reservoir. The Vp/Vs ratio is limited to ≥ 1.85, indicating water-saturated regions in the reservoir. As seen in the map view (Figure 22a), the high Vp/Vs values are concentrated below the locations of several water injectors from which a narrow trail meanders towards the SCF, where the water appears to pool. Figure 22b shows a cross sectional view of the data from east to west. The SCF is represented by the southwestward dipping planar structure along the left margin of the figure, while the other light-colored subvertical planes denote faults and fractures in the reservoir. The high Vp/Vs anomaly conforms to the dipping fault, representing the pooling of water where flow is inhibited by the impervious fault. In fact, this Vp/Vs anomaly is identical to an anomaly reported by Gritto et al. (2013b).

Figure 22: Delineation of Flow Path via High Vp/Vs-Ratio

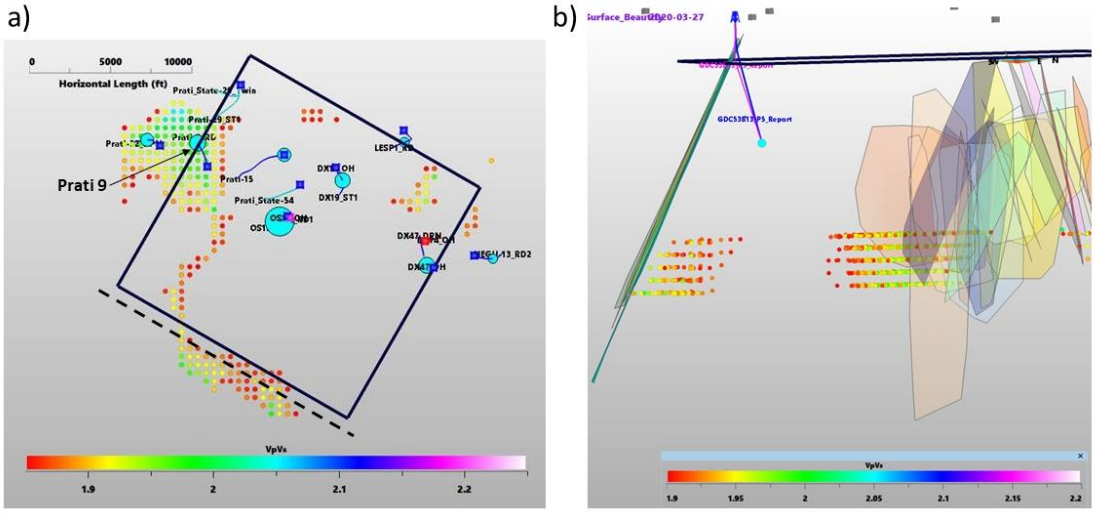

(a) Map view at 2,440 m depth, showing the Vp/Vs ratio ≥ 1.85 illustrating a flow path of water from the location of water injector Prati 9 (cyan-colored disc located along northwestern boundary of study area) towards the Big Sulphur Creek fault (dashed line along southwestern boundary of the study area). The 5x5 km study area is denoted by the black square. (b) Vertical view from east to west, of the high Vp/Vs anomaly below the southwestward dipping trajectory of the Big Sulphur Creek fault. Subvertical light-colored planes represent projections of inferred fracture and fault planes in the reservoir. The colored dots represent Vp/Vs estimates resulting from the 3D velocity inversion at 150 m node spacing.

Source: Lawrence Berkeley National Laboratory

Figure 23 presents the full scale of Vp/Vs estimates at 2,440 m depth. The map shows the Vp/Vs estimates by colored dots, while the top-of-steam surface, representing the top of the reservoir, is indicated by the colored contour lines with warmer to colder colors representing shallower to deeper levels, respectively. As before, the flow path of water from the Prati 9 injector to the SCF is indicated by the high Vp/Vs values. Furthermore, the narrow distance between the steam contours in the area of the SCF indicates its steep dip towards the southwest. Low Vp/Vs estimates are mainly concentrated in the center of the study and below

steam contours. The sharp contrast of the high Vp/Vs anomaly in the vicinity of the Prati injection wells and the low Vp/Vs anomaly immediately to the south indicates that the reservoir is highly compartmentalized as will be shown below. In general, the results suggest that Vp/Vs is a good indicator for both water-saturated zones and fluid flow path as well as concentration of steam in the reservoir. However, the contour lines in Figure 23 represent different depth levels and are only projected onto the map at 2,440 m depth.

Figure 23: Spatial Distribution of Vp/Vs-Ratio

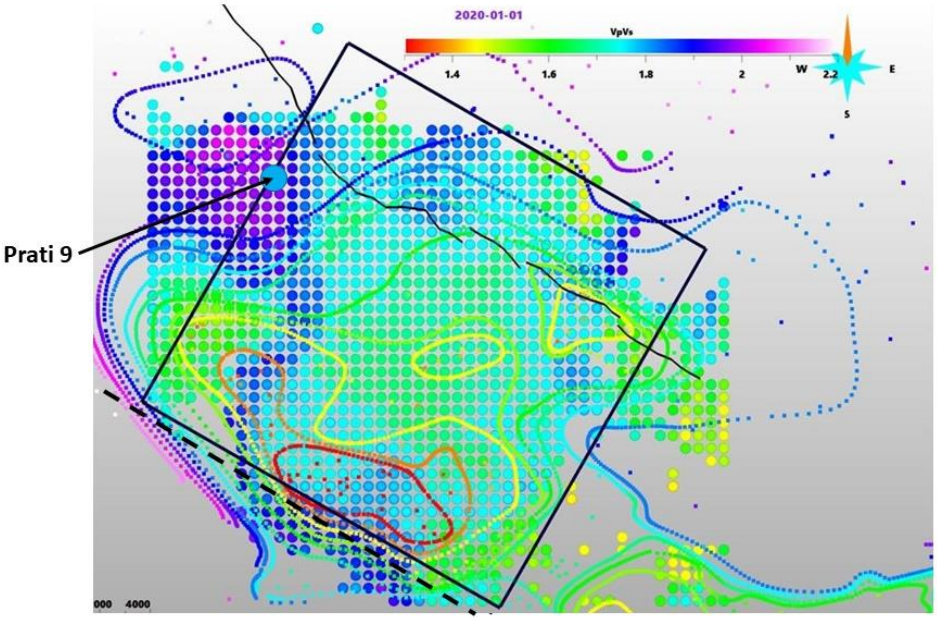

Map view of the full scale Vp/Vs ratio at 2,440 m depth. The contour lines represent the top-of-steam surface, with warmer to colder colors representing shallower to deeper levels, respectively. Black solid lines represent the surface traces of a fault inferred from hypocenter locations of seismicity at depth. The 5 km x 5 km study area is denoted by the black square. The colored dots represent Vp/Vs estimates resulting from the 3D velocity inversion at 150 m node spacing. The dashed line on the southeastern boundary of the study are represents the approximate surface location of the Big Sulphur Creek Fault.

Source: Lawrence Berkeley National Laboratory

Figure 24a and 24b present the shear modulus at depths of 720 m and 1220 m, respectively. The maps point to a feature referred to by Calpine as the "dead zone," a region with more competent Graywacke that is less fractured and contains fewer steam entries. Calpine has been unsuccessful in finding steam in this part of the reservoir. The dead zone is delineated by a set of two orthogonally oriented faults in the southeastern corner of the study area (labeled "1"). As can be seen in Figure 24, this area is defined by high shear moduli ranging from 33–40 gigapascals (GPa). The maps show the lateral extent of this zone, defined by the two bounding faults. The shear modulus of the rock drops noticeably beyond the boundaries of the faults. This example shows the resolution and imaging capabilities of the high-density seismic station network in defining the structural controls of the reservoir. The flow path of water from the Prati 9 injector to the SCF that was indicated by the high Vp/Vs values in Figure 22 and Figure 23, is manifested by low shear moduli, ~ 20 GPa, at the 1,220 m depth level in Figure 24b. Low shear moduli are typically associated with fractured rock which increases permeability and provides a pathway for the water to flow through the reservoir. Thus, the low

shear modulus indicates the cause of the water flow path (fractured rock) and the high Vp/Vs indicates the effect (fluid flow through the reservoir).

Figure 24: Spatial Distribution of Shear Moduli

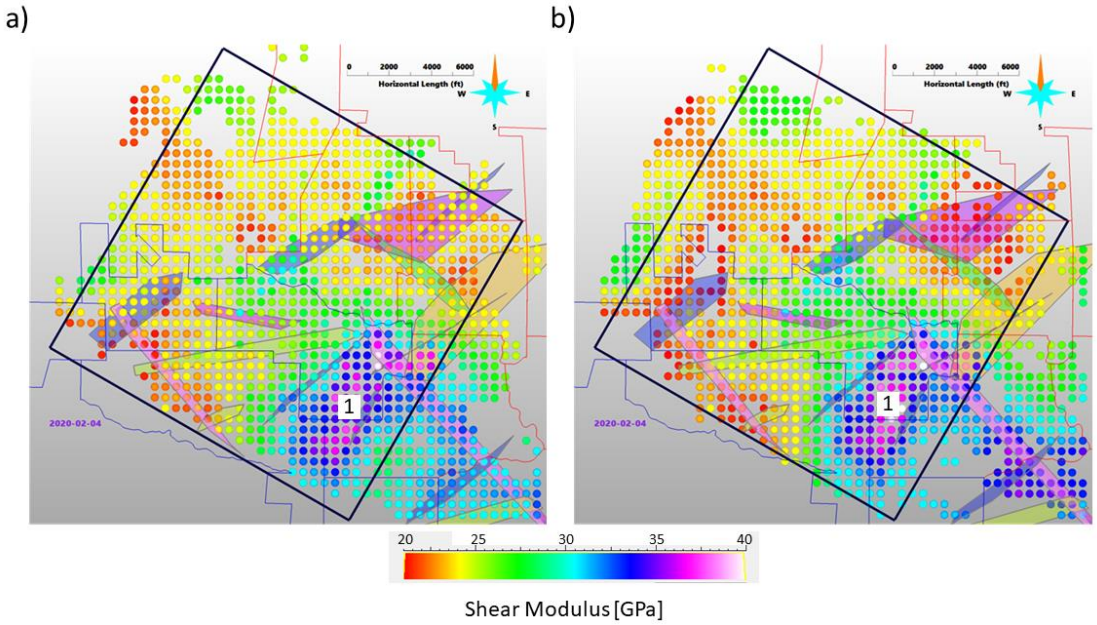

(a) Map view of shear modulus at 720 m depth. The light-colored planes represent projections of inferred fracture and fault planes in the reservoir. The thin lines represent boundaries of leases in the reservoir. (b) Map view of shear modulus at 1,220 m depth. The colored dots represent estimates of the shear modulus resulting from the 3D velocity inversion at 150 m node spacing. The dead zone, a region with more competent Graywacke that is less fractured and contains fewer steam entries is indicated by the label "1".

Source: Lawrence Berkeley National Laboratory

Figure 25 shows a cross section through the reservoir denoting the major geological formations and associated rock types. The figure delineates the interfaces between the major rock types (black dashed lines), the top of the steam (brown dashed line) and the trajectory of boreholes superimposed with the lithologies (color coded). Steam entries are denoted by red discs along the borehole trajectories. In the "dead zone," a paucity of steam entries exists along the wells, while in more productive areas of the reservoir the steam entries are found ubiquitously as soon as the depth reaches the top of steam boundary. While the dead zone is composed of competent Graywacke that contains few fractures, the productive areas of the reservoir comprise Argilliceous Graywacke that reveals a higher degree of fracturing.

Figure 25: Cross Section of Major Geological Formations

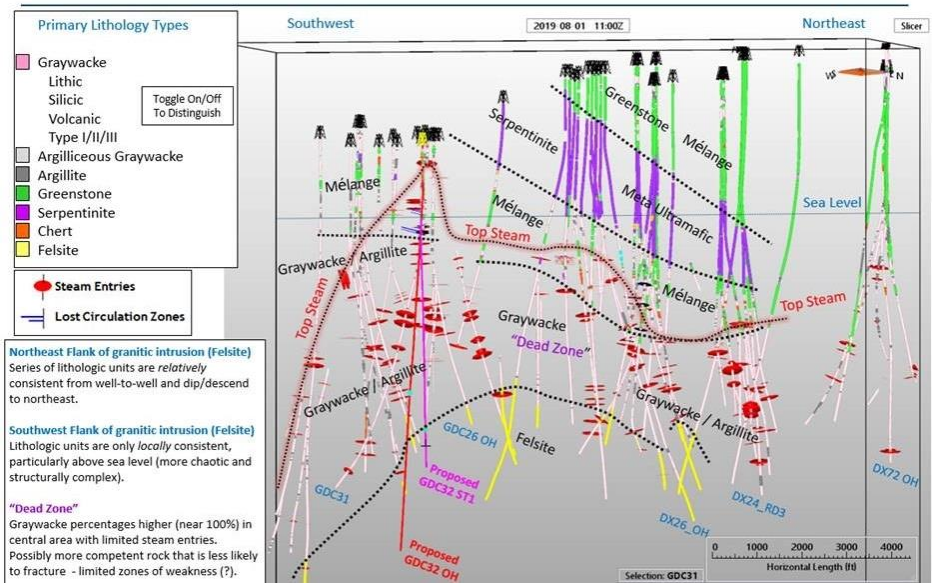

Cross section through The Geysers reservoir showing the major geological formations and associated rock types, the top of steam surface and trajectory of boreholes. The "Dead Zone" is represented by an area with compact Graywacke, while steam-producing regions are composed of Graywacke, Argillite and Argilliceous Graywacke. Red discs along boreholes denote steam entries. Note the paucity of steam entries along the wells in the dead zone.

Source: Lawrence Berkeley National Laboratory

Main features of Calpine's reservoir model (for example, Hartline et al., 2019) are fault and fracture surfaces that have been delineated from the analysis of double-difference hypocenter locations (Waldhauser and Ellsworth, 2000). However, thus far researchers have not attempted spatial correlation to seismic velocities or elastic moduli to support this fault and fracture analysis. This issue is addressed in Figure 26, which presents the S-wave velocities at 2,130 m depth. The S-wave velocities are indicated by the colored dots, while the faults and fractures, inferred from earthquake hypocenters, are denoted by the colored linear features. Some of the anomalies in Figure 26 are annotated to support the discussion of the reservoir structure in the following. Anomaly 1 denotes the dead zone shown in Figure 24 and Figure 25. The shear wave velocity is high as expected for competent rock. As for the shear modulus in Figure 24, the high velocities are clearly bounded by the surrounding faults. Anomalies 2a, 2b and 2c are composed of intermediate to low S-wave velocities (green colored dots), are bounded by the brown and gray colored faults on their southwestern flank, and nicely follow the stepover of the faults in northwesterly direction. Anomalies 3 and 4 are also clearly separated by the fault or fracture zone denoted by the purple, light blue, and orange symbols traversing in southwest-to-northeasterly direction. Finally, anomalies 3 and 5 are separated by the gray-colored fault striking southeast to northwest. Node spacing during the seismic travel time inversion was 150 m, which greatly improves the resolution of the resulting images as demonstrated in Figure 26.

Figure 26: Cross Section of Major Geological Formations

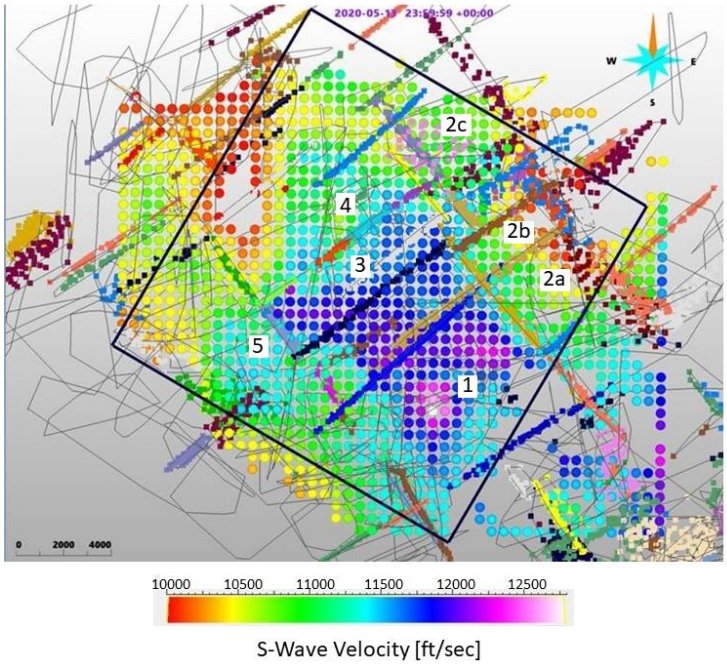

Map with S-wave velocities at 2,130 m depth. Linear colored features represent faults and major fracture zones inferred from earthquake hypocenters. The study area is indicated by the black square. The colored dots represent Vs estimates resulting from the 3D velocity inversion at 150 m node spacing.

Source: Lawrence Berkeley National Laboratory

The dense seismic network deployed at The Geysers geothermal reservoir enabled unprecedented advances in large-scale seismic imaging by improving the resolution of the resulting velocity estimates to previously unrealized levels. As shown in the figures, the obtained images are essential in supporting the interpretation of the structural reservoir features and have already improved Calpine's confidence in the tomographic inversion results that will support and improve its future drilling program.

CHAPTER 4:
Technology Transfer Activities

Purpose

This plan describes how the knowledge and innovations advanced by this project are made available to the public, including geothermal field operators (Calpine, U.S. Geothermal Community), utilities (for example, Pacific Gas and Electric Company), government agencies (California Geologic Energy Management Division [CalGEM], USDOE GTO), and geophysicists and local communities (such as Geysers Seismic Monitoring Advisory Committee).

The overarching plan is to communicate the lessons from this project at technical and geothermal industry conferences and in peer-reviewed scientific journals. Through the course of the project, the research team worked closely with Calpine Corp, provided regular status reports, and made the data, images, analyses, reports, and presentation materials available. The research team also communicated the results of this work to USDOE's GTO.

Most of all, the research team shared the results with Calpine Corp. the operator of The Geysers geothermal reservoir for incorporation into its 3D geothermal reservoir model and use in its borehole planning program.

The technology developed under this project is also offered by JDS to the geothermal industry in California and the U.S., and to international stakeholders.

Intended Use of Gained Knowledge and Developed Technology

A key technological challenge required for the growth of geothermal energy is to "better understand the influence of major fractures and faults as subsurface barriers or conduits to flow" (MIT-led interdisciplinary panel, 2006). Imaging of flow paths, barriers and heterogeneity in geothermal reservoirs is critical because efficient production of steam typically requires injected water to supplement the geothermal resource naturally replenished by rainwater or snowmelt. The ability to spatially visualize the major conduits for the transport of water and steam during injection and production is critical to ensure cost-effective operation and development of the geothermal resource.

This project advanced the current ability to image subsurface flow paths, barriers, and heterogeneity in operating geothermal reservoirs through an integrated approach that combines the recent development of low-cost, dense seismic networks together with established state-of-the-art micro-earthquake imaging. The technology has general utility for quantifying the response of an operating geothermal field to changes in injection and production, including understanding the impact of flexible (non-baseload) geothermal generation, required for grid operation with higher levels of wind and solar. The relationships between seismic imaging results and reservoir properties developed in this project can equally be applied by technical geoscientists working for geothermal operating companies and by geophysical service providers.

Publications

The research results were reported at scientific conferences during the project. Researchers presented two papers at the Stanford Geothermal Workshop and three papers at the American Geophysical Union Annual Meeting:

- Gritto, R., L.J. Hutchings, S. Jarpe, K.T. Nihei, M. Schoenball (2020), Seismic Imaging of Spatial- and Temporal Heterogeneity of a Geothermal Reservoir Using a Cost-Effective Dense Seismic Network, Proceedings, 45th Workshop on Geothermal Reservoir Engineering, Stanford University, Stanford, California, February 10-12, 2020, SGP-TR-215.
- Gritto, R., S. Jarpe, L.J. Hutchings, K.T. Nihei, M. Schoenball, C.S. Hartline (2019), High-Resolution Imaging of Geothermal Flow Paths Using a Cost-Effective Dense Seismic Network, S11F-0393, Proceedings AGU 2019 Fall Meeting, San Francisco, CA, Dec. 9-13, 2019.
- Layland-Bachmann, C.E., R. Gritto, C.S. Hartline, L.J. Hutchings., S.R. Jarpe, K.T. Nihei and M. Schoenball (2019), S11F-0394, In-depth Analysis from Deployments of Low-Cost Seismic Instruments in the Geysers Geothermal Field, Proceedings AGU 2019 Fall Meeting, San Francisco, CA, Dec. 9-13, 2019.
- Gritto, R., D.W. Vasco L.J. Hutchings, K.T. Nihei (2019), High-Resolution Seismic Imaging of a Geothermal Reservoir Using a Cost-Effective Dense Seismic Network, Proceedings, 44th Workshop on Geothermal Reservoir Engineering, Stanford University, Stanford, California, February 11-13, 2019, SGP-TR-214.
- Gritto, R., D.W. Vasco L.J. Hutchings, K.T. Nihei (2018), A Network Design Study for Optimum Resolution of Reservoir Parameters Based on a Dense Seismic Array at The Geysers Geothermal Reservoir, CA S33C-0590, Proceedings AGU 2018 Fall Meeting, Washington D.C., Dec. 10-14, 2018.

Copies of Documents

The project team submitted copies of all technical reports to the CEC and made papers and abstracts of the publications listed above publicly available on the respective webpages of the conference organizers.

Use in Policy Development

At this time, the researchers do not anticipate that project results will be used to develop government policy or inform regulatory agencies.

Public Requests for Project Results

The research team will record the number and source of all requests made for project documents.

Technology Transfer

The immediate results of the project are presently being used by Calpine Corp., the operator of The Geysers geothermal reservoir, to inform its drilling program in the study area. The

program envisions the drilling of new wells and the reopening and deepening of abandoned wells to improve production in the area.

The near-term market of the developed technology is its application to The Geysers, where the deployed seismic network is still operating. Calpine has already signaled its willingness to take over the network and continue future operations. Calpine has incorporated the derived 3D velocity and elastic moduli models into its 3D reservoir model that will guide their drilling operations into the future. The mid-term target markets include geothermal reservoirs in California, including the Coso and Salton Sea geothermal fields. Both fields reveal induced seismicity, which can be used to perform the seismic imaging conducted in this project. Long-term markets of this technology include geothermal reservoirs outside California, such as new developments in Cascadia (northwestern United States), Nevada, Idaho, Utah, and Hawaii where planned enhanced geothermal systems are expected to generate induced seismicity. Additionally, international markets could include geothermally productive regions such as Iceland, Turkey, Taiwan, the Philippines, Indonesia, and New Zealand.

JDS codeveloped the technology and offers this service to operators in California, the U.S., and abroad. JDS will continue to market this technology. During the presentations of the results at scientific conferences the research team was approached by several stakeholders interested in using the low-cost seismic sensors at their geothermal operations.

At present, the developed technology is coupled with magneto telluric sounding, another geophysical imaging technique, to improve the reliability of the resulting reservoir images.

The successful application of this technology at The Geysers has already resulted in Calpine Corp. embracing the results of the project to inform on the planning of their drilling program. This is an important first step, which proves that seismic imaging can be used to improve reservoir operations. JDS can use examples of the research results to promote this technology to other stakeholders.

By proving that this technology can be used to image the processes and heterogeneity in a geothermal reservoir, governmental agencies and public regulators are more likely to promote the development of enhanced geothermal systems, which can be difficult to manage because knowledge of the generated fracture network relies on the availability remote sensing techniques.

CHAPTER 5: Conclusions

The primary goals of this project included the development of an advanced, low-cost, automated tomographic imaging system that uses micro-earthquakes to form high spatial resolution images of subsurface fluid flow, flow barriers and heterogeneity in producing geothermal fields, and the demonstration of the practical implementation of this technology in an operating geothermal field. The technical advancement of this project included integration of these components into a system that can be cost-effectively, reliably and routinely deployed in operating geothermal fields to image the movement of fluids in the reservoir with a fast-turnaround time from data collection, to processing, to imaging, and to rock physics interpretations. The effort focused on micro-earthquake imaging challenges that are unique to geothermal reservoirs that can include complex fracturing and faulting, heterogeneous overburden and limited seismic velocity control. The product of this project will enable geothermal operators to carry out their operations more efficiently by drilling productive wells, avoiding drilling hazards, and optimizing production.

The researchers envisioned the low-cost seismic network to operate autonomously at geothermal reservoirs over extended periods of time, a requirement that is currently not met by other low-cost seismic sensors. With its internal battery and a solar panel for power supply as well as memory cards for data storage, the size of the memory cards determines the limit in operation time between service intervals. The low-cost seismic recorders in this project have the option to include cell phone boards for automatic data transmission, which the researchers recommend if cell phone coverage exists in the field. Transmission rates of inexpensive cell phone service are high enough for data volumes generated by the recording of micro-seismicity (for example, 200 samples per second). The researchers further recommend adding metal fins to the outside of the sensor housing to improve shear coupling to the ground.

Numerical modeling of the resolution of high-density seismic network geometries suggested the resolution to be largely independent of sensors locations. This is particularly useful for deployment in terrains where regular spacing of sensors is impractical due to steep topography or thick foliage preventing clear views of the sky for solar power. However, when the number of seismic stations in a network becomes too low, comparable resolution for the regular-spaced versus randomly-spaced network design is no longer given. In this case, a regular-spaced network design yields the higher resolution for the P- and S-wave estimates in the reservoir.

Lower seismicity rates may decrease the resolution of the P- and S-wave velocities in the reservoir. However, increasing the number of seismic stations at the surface can somewhat mitigate this limitation, which may be particularly appealing for region such as the Basin and Range province, which exhibits low levels of natural seismicity.

Vp/Vs ratio is a good indicator for water and steam saturation. If water injection and steam production rates are known, for example as functions of depth in boreholes, the surrounding Vp/Vs estimates can be calibrated by the respective water injection or steam production

volumes. This will aid in the interpretation of Vp/Vs estimates in the reservoir where borehole information is unavailable.

The combination of Vp/Vs ratio, P- and S-wave velocities and elastic moduli, such as shear modulus, combined with reservoir data derived from observations in boreholes, such as fault and fracture surfaces, water injection and steam production volumes, fracture densities, and so on allow interpretation of the seismic images in terms of water and steam saturated zones, fluid pathways, flow barriers, and fractured/solid competent rock. This information allows the operator of the reservoir to develop a better drilling program minimizing the drilling of unsuccessful wells.

CHAPTER 6:
Benefits to Ratepayers

California Senate Bill (SB) 350 established a statewide goal of 50 percent electricity generation from renewable sources by 2030. Continued growth of California's broad portfolio of renewable energy, including geothermal, is required to achieve the goals of SB 350. This growth can be accelerated through the development of innovative technologies and by narrowing the gap of these technologies to commercialization. A key technological challenge required for the growth of geothermal energy is to "better understand the influence of major fractures and faults as subsurface barriers or conduits to flow" (MIT-led interdisciplinary panel, 2006). Imaging of flow paths, barriers and heterogeneity in geothermal reservoirs is critical because efficient production of steam typically requires injected water to supplement the geothermal resource naturally replenished by rainwater or snowmelt. The ability to spatially visualize the major conduits for the transport of water and steam during injection and production is critical information to ensure cost-effective operation and development of the geothermal resource.

This project advanced the current ability to provide images of subsurface flow paths, barriers, and heterogeneity in operating geothermal reservoirs through an integrated approach that combines the recent development of low-cost, dense seismic networks together with established state-of-the-art micro-earthquake imaging. The technology has general usefulness for quantifying the response of an operating geothermal field to changes in injection and production — including understanding the impact of flexible (nonbaseload) geothermal generation — required for grid operation with higher levels of wind and solar.

The results of the current project are important to the California ratepayers because they will help Calpine Corp. optimize reservoir operations at The Geysers geothermal reservoir, the largest geothermal reservoir in the world that provides approximately 850 MW of electricity to ratepayers in northern California.

The results provide important information to Calpine Corp. that can be used in planning its drilling program. In the study area, a recently drilled production well turned out dry and was subsequently converted to a water injection well. Such situations increase the total cost of Calpine's drilling program without generating additional electricity. After results from the developed technology became available, Calpine incorporated them into its 3D geothermal reservoir model, which has already aided in the planning of future wells. The cost of a geothermal well can be as high as $6.5 million per borehole so assisting with successful completion of the production and water injection wells will reduce the overall cost of drilling and thus reduce the electricity rates for California ratepayers. An improvement in steam recovery and water injection efficiency of about 5 to 10 percent is realistic, based on the results of this project. If this project improves efficiency by 5 percent, the annual savings at The Geysers would amount to $560,000. An improvement of 10 percent would provide annual savings of $825,000. These figures include the savings in purchasing and operating the low-cost seismic network over similar competitive networks at $280,000/year. While the developed technology can be successfully operated as a stand-alone tool, a new research project is

currently further refining the technology by coupling it with magneto telluric sounding, another geophysical imaging technique, to improve the reliability of the resulting images of the reservoir structure.

Steam Production Increase

The resource of a geothermal reservoir is the amount of heat that can be mined to generate electricity. In a dry steam dominated reservoir, such as The Geysers, the hot steam that is produced is driving turbines generating electricity at the local powerplants. Thus, an increase in steam production at constant or reduced costs will result in an increase in generated electricity, which is a benefit to the California rate payer.

The average Geysers well encounters a limited number of productive steam entries (3-7), and researchers anticipate improved subsurface resolution to allow refined targeting and encounter additional steam entries. The research team estimated the value of an incremental steam production increase due to refined well targeting within the proposed study area, based on known values of the (1) average steam production rate, (2) pipeline interference, (3) steam flow rate to electricity production, and (4) electricity production to dollars. Table 2 shows a range of percent increases in incremental steam production that could be reasonably anticipated by improved subsurface resolution and the resulting refined well targeting, and provides the associated present value and earnings before interest, taxes, depreciation, and amortization/year (EBITDA/Year) for each case.

Table 2: Increases in Incremental Steam Production by Improved Well Targeting

Unit 7/8 Estimates (at center of proposed study area)	Con-stants	Incremental Steam Production Improvement With Refined Well Targeting									
Average Steam Production Rate (lb/hr)	**36,180**										
Production Improvement (%)		**1%**	**2%**	**3%**	**4%**	**5%**	**6%**	**7%**	**8%**	**9%**	**10%**
Production Improvement (lb/hr)		362	724	1,085	1,447	1,809	2,171	2,533	2,894	3,256	3,618
Pipeline Interference (%)	**50**										
Production Improvement (lb/hr) w/50% Interference		180.9	361.8	542.7	723.6	904.5	1,085.4	1,266.3	1,447.2	1,628.1	1,809.0
Incremental Steam Rate (lb/kWh)	**15.5**										
Production Improvement (kW) w/50% Interference		12	23	35	47	58	70	82	93	205	117
Production Improvement ($) w/50% Interference											
Present Value, 5 years, 9%, after-tax		**$12,991**	**$25,982**	**$38,973**	**$51,964**	**$64,955**	**$77,946**	**$90,937**	**$103,928**	**$116,920**	**$129,911**
EBITDA* per year		$6,149	$12,298	$18,447	$24,596	$30,745	$36,893	$43,042	$49,191	$55,340	$61,489
EBITDA* per year		**$30,745**	**$61,489**	**$92,234**	**$122,978**	**$153,723**	**$184,467**	**$215,212**	**$245,956**	**$276,701**	**$307,446**

*** Earnings Before Interest, Taxes, Depreciation, and Amortization**

Source: Lawrence Berkeley National Laboratory

Water Injection Increase

Geothermal operators use water injection to sustain the resource of the reservoir. However, at present only a fraction of the injected water is recovered as steam. If the siting of water injection wells can be optimized, recovery rates will increase resulting in an increase in generated electricity, which benefits the California rate payer.

Water injection wells also depend on encountering the same steam entries (fracture systems) and would also benefit from improved well targeting. Although the relationships between water injection and increased steam production are less direct, it is understood that approximately 30 percent to 40 percent of the injected water mass is recovered as steam production (peaking 2-3 years after water injection is initiated due to injector-producer separations). Researchers anticipate values similar to those shown for incremental steam production increases.

Drilling Cost Reduction

The cost of drilling steam production or water injection wells is the single most expensive component in the operation of a geothermal reservoir. The heat and the heterogeneity of the volcanic reservoir rocks result in much higher cost compared to drilling for oil or gas in sedimentary reservoirs. Providing reliable information on the drilling target at depth reduces the risk of dry or unsuccessful wells, which lowers drilling cost and thus lowers the cost of the generated electricity, which benefits the California rate payer.

At The Geysers, the drilling program (both water injection and steam production) is designed for sustainability of the resource at approximately the existing steam production level. New Geysers "deep" wells are drilled to an average target depth of 8,500-9,000 feet, take about 85 days to drill, and cost approximately $6.5 million, while new Geysers shallow low-rate injection (SLRI) wells are drilled to approximately 3,500-4,000 feet and cost approximately $3 million to drill. The Geysers well drilling program depends heavily on yearly budgets, but generally includes, at minimum, the equivalent of two new deep wells and one new SLRI well (or the equivalent of 10 deep wells and 5 SLRI wells in 5 years). There is also a significant drilling budget for well recompletions, sidetracks, deepened wells, and conversion-to-injection. The total drilling cost assigned for the 15 new wells over 5 years (in 2016 dollars) is approximately $80 million.

In the extreme case, if a well were able to provide twice the average steam production or were able to allow twice the water recharge, a well could be eliminated from the drilling budget. More realistically, drilling several wells with a 5 percent to 10 percent efficiency increase (whether in steam production or water injection reservoir recharge) is a reasonable assumption with improved well targeting. At a 5 percent efficiency increase, 1 well in 20 could be eliminated from the drilling program. At a 10 percent efficiency increase, 1 well in 10 could be eliminated from the drilling program. The proposed study area is 25 km^2, or slightly more than 25 percent of The Geysers productive steam reservoir area (with an area of approximately 1.02513×10^9 ft^2 or about 95 km^2). Researchers therefore expect that this study would affect approximately 25 percent of The Geysers wells. Table 3 shows the potential impact on the drilling budget with slightly improved well targeting.

Table 3: Impact on Drilling Budget by Improved Well Targeting

Item	Cost	Percent Improvement in Steam Production or Water Injection Per Well Provided By Improved Resolution of: (1) Fluid Flow path, (2) Fluid Boundaries, (3) Reservoir Heterogeneity and (4) Reservoir Compartmentalization									
Percent Improvement		**1%**	**2%**	**3%**	**4%**	**5%**	**6%**	**7%**	**8%**	**9%**	**10%**
New Deep Injection Well	**$6,500,000**	$65,000	$130,000	$195,000	$260,000	$325,000	$390,000	$455,000	$520,000	$585,000	$650,000
New Deep Steam Production Well	**$6,500,000**	$65,000	$130,000	$195,000	$260,000	$325,000	$390,000	$455,000	$520,000	$585,000	$650,000
New Shallow Low-Rate Injection (SLRI) Well	**$3,000,000**	$30,000	$60,000	$90,000	$120,000	$150,000	$180,000	$210,000	$240,000	$2,700,000	$300,000
Total Drilling Cost for Three New Wells	**$16,000,000**										
Potential One Year Drilling Cost Reduction (100% Geysers)		$160,000	$320,000	$480,000	$640,000	$800,000	$960,000	$1,120,000	$1,280,000	$1,440,000	$1,600,000
For Study Area: Potential One Year Drilling Cost Reduction (25% Geysers)		$40,000	$80,000	$120,000	$160,000	$200,000	$240,000	$280,000	$320,000	$360,000	$400,000
For Study Area: Potential Five Year Drilling Cost Reduction (25% Geysers)		$200,000	$400,000	$600,000	$800,000	$1,000,000	$1,200,000	$1,400,000	$1,600,000	$1,800,000	$2,000,000

Source: Lawrence Berkeley National Laboratory

Tracer Study Reduction

The Geysers budgets around $50,000 per year for tracer studies to better understand reservoir fluid flow. The improvements in imaging technology provided by this project, specifically the detailed analysis of the spatial relationship between water injection and imaged seismic velocities, provide a strong correlation in fluid flow determinations between seismic imaging and tracer studies. With sufficient subsurface resolution, it is realistic to assume elimination of 30 percent to 50 percent of future tracer studies for a savings of approximately $75,000 to $125,000 over five years.

Development of Low-Cost Seismic Station

During this project, Jarpe Data Solutions, Inc. further developed a prototype of a low-cost seismic station for field operations that was subsequently deployed at The Geysers geothermal reservoir. The low-cost seismic station includes a 12-V battery, an electric circuit board, three orthogonally oriented 4.5 Hz geophones, a GPS antenna, a 24-bit digitizer, two memory SD card slots and allows for continuous data recording. The design of the seismic station also supports real-time data transmission via an internal cell-phone card. However, because of the lack of cell phone coverage at The Geysers geothermal reservoir, this project did not implement real-time data submission. The seismic station is complemented by a 10-W solar panel, externally mounted on top of the station that allows for continuous operation. The cost of the developed seismic station is $1,000 per unit.

Oyo Corp. and NodalSeismic offer comparable seismic stations, but these units do not offer continuous data recording because they lack an external solar panel, while their internal batteries only support approximately two weeks operation. Despite these shortcomings, these comparable stations cost $3,000 per unit. In addition, due to lack of solar power these units would require biweekly visits at a cost of $3,600 per visit or $93,600 per year. Finally, use of these comparable stations by either Oyo Corp. or NodalSeismic would cost $300,000, for a total annual operating cost of $393,600.

In contrast, for the current project at The Geysers, the research team installed a dense network of low-cost sensors in a 5 km x 5 km study area. Monitors visit the current stations quarterly for data retrieval at a cost of $3,600 per visit or $14,400 per year. Deployment of a dense seismic network with 100 low-cost stations would amount to $100,000, so total operating costs for one year using the low-cost seismic stations in this project are $114,400. Therefore, total savings using the low-cost seismic station would amount to $279,200 for the operation of a 100-station seismic network for one year. The low-cost stations are available to geothermal operators in California through Jarpe Data Solutions, Inc.

Table 4: Operation Cost of 91-Station Seismic Network

Offerer	Seismic Station	100-Station Network	Service/ Visit	Service/ Year	Total	Total Savings
Jarpe Data Solution , Inc.	$1,000	$100,000	$3,600	$14,400	$114,400	$0
Oyo Corp.	$3,000	$300,000	$3,600	$93,600	$393,600	$279,200
NodalSeismic	$3,000	$300,000	$3,600	$93,600	$393,600	$279,200

Source: Lawrence Berkeley National Laboratory

LIST OF ACRONYMS

Term	Definition
AIT	Array Information Technology
EBITDA	Earnings Before Interest, Taxes, Depreciation, and Amortization
CEC	California Energy Commission
cm	Centimeter
GPa	Gigapascal
GPS	Global Positioning System
GTO	Geothermal Technology Office
GW	Gigawatt
Hz	Hertz
JDS	Jarpe Data Solutions
kg	Kilogram
km, km^2	Kilometer, Square Kilometer
l	Liter
LBNL	Lawrence Berkeley National Laboratory
m	Meter
ms	Millisecond
Mw	Moment Magnitude
mW	Milliwatt
MW	Megawatt
NCEDC	Northern California Earthquake Data Center
SB	Senate Bill
SCF	Sulphur Creek Fault
SD	Secure Digital
SEGEP	South East Geysers Effluent Project
SLRI	Shallow Low-Rate Injection
sps	Samples per Second
SRGRP	Santa Rosa Geysers Recharge Project
3D	Three Dimensional

Term	Definition
U.S.	United States
USDOE	United States Department of Energy
VDC	Voltage Direct Current
Vp	P-wave Velocity
Vs	S-wave Velocity
W	Watt

REFERENCES

Adams D. A., and Abercrombie R. E., (1998), Seismic attenuation above 10 Hz in southern California from coda waves recorded in the Cajon Pass borehole, J. Geophys. Res., 103, 24,257–24,270.

Allis, R.G., (1982), Mechanism of induced seismicity at The Geysers geothermal reservoir, California, Geophysical Research Letters, 9, 6, 629-632.

Allis, R. and Shook, G.M., (1999), An alternative mechanism for the formation of The Geysers vapor-dominated reservoir, Proceedings of the 24th Workshop on Geothermal Reservoir Engineering, Stanford, SGP-TR-162.

Boitnott, G.N., (1995), Laboratory measurements of reservoir rocks from The Geysers geothermal field. Proceedings, 20th Workshop on Geothermal Reservoir Engineering, Stanford University, SGP-TR-150, 107–114.

Boitnott, G.N., and P.J. Boyd, (1996), Permeability, electrical impedance, and acoustic velocities on reservoir rocks from The Geysers geothermal field. Proceedings, 21st Workshop on Geothermal Reservoir Engineering, Stanford University, SCP-TR-151, 343–350.

Boyle, K., Jarpe, S., Hutchings, L., Saltiel, S., Peterson, J. and Majer, E., (2011), Preliminary investigation of an aseismic 'doughnut hole' region in the northwest Geysers, California, Proceedings of the 36th Workshop on Geothermal Reservoir Engineering, Stanford, SGP-TR-191.

Brikowski, T.H., (2001), Deep fluid circulation and isotopic alteration in The Geysers system: profile models, Geothermics, 30, 333-347.

Brocher, T.M., (2005), Empirical relations between elastic wave speeds and density in the Earth's crust, *Bull. Seism. Soc. Am.*, 95(6), 2081–2092, doi: 10.1785/0120050077.

Bufe, C.G., Marks, S.M., Lester, F.W, Ludwin, R.S. and Stickney, M.C., (1981), Seismicity of The Geysers-Clear lake region, U.S. Geological Survey Professional Paper, 1141, 129-137.

California Department of Conservation, Division of Mines and Geology, Open File Report 96-08, U.S. Department of the Interior, U.S. Geological Survey Open-file Report 96-706, Appendix A, California Fault Parameters.

Crowell, J.C., (1974), Origin of late Cenozoic basins in southern California, Soc. Econ. Paleontologists Mineralogists Spec. Pub., 22, 190-204.

Donnelly-Nolan, J.M., Burns, M.G., Goff, F.E., Peters, E.K. and Thompson, J.M., (1993), The Geysers-Clear lake area, California: Thermal waters, mineralization, volcanism, and geothermal potential, Economic Geology, 88, 310-316.

Eberhart-Phillips D., (1986), Three-dimensional Velocity Structure in Northern California Coast Ranges from Inversion of Local Earthquake Arrival Times, Bul. Seis. Soc. Am. 76, No. 4, pp. 1025-1052.

Eberhart-Philips, D. (1988), Seismicity in the Clear Lake area, California, Geological Society of America Special Paper, 214, 195-206.

Eberhart-Phillips, D., M. Reyners, M. Chadwick, J.M. Chiu, (2004), Crustal heterogeneity and subduction processes: 3-D Vp, Vp/Vs and Q in the southern North Island, New Zealand, Geophys. J. Int., 162, 1, 270–288.

Dreger, D.S., R. Gritto, O.S. Boyd, and T. Taira, 2018, Seismic Analysis of Spatio-Temporal Fracture Generation at The Geysers EGS Demonstration Project, Proceedings, 43rd Workshop on Geothermal Reservoir Engineering, Stanford University, Stanford, California, February 12-15, 2018, SGP-TR-213, pp. 1-13.

Gardner, G.H.F., L.W. Gardner, and A.R. Gregor, (1974), Formation velocity and density – The diagnostic basics for stratigraphic traps, *Geophysics*, Vol. 39, No. 6, pp. 770–870.

Gentili, S. and G. F. Gentile, (2015), High frequency attenuation k parameter and QS 3D model for South-Eastern Alps and North-Western Dinarides, Bollettino di Geofisica Teorica ed Applicata, in press.

Gladwin M.T., F.D. Stacey, (1974), Anelastic degradation of acoustic pulses in rock, Phys. Earth Plan. Int., 8, 4, 332-336.

Gritto, R., S.H. Yoo and S.P. Jarpe, (2013a), 3D Seismic Tomography at The Geysers Geothermal Field, CA, USA, Proceedings of Thirty-Eighth Workshop on Geothermal Reservoir Engineering, Stanford University, Stanford California, 11-13 February, 2013, SGP-TR-198. Pp.1-12.

Gritto, R., S.H. Yoo and S.P. Jarpe, S., (2013b), Seismic Imaging of reservoir structure at The Geysers geothermal reservoir, in AGU Fall Meeting 2013 S33D-2460, San Francisco, USA, 9–13 December 2013.

Gritto, R., and S.P. Jarpe, (2014), Temporal variations of Vp/Vs ratio at The Geysers geothermal field, USA, Geothermics, Vol. 52, 112–119, http://dx.doi.org/10.1016/j. geothermics.2014.01.012.

Gritto, R., D.S. Dreger, O.S. Boyd, and T. Taira, (2016), Fluid Imaging, Moment Tensors and Finite Source Models During the EGS Demonstration Project at The Geysers, CA, Proceedings of Forty-First Workshop on Geothermal Reservoir Engineering, Stanford University, Stanford CA, February, 22-24, 2016, SGP-TR-209, pp. 1-12.

Gritto, R., L.J. Hutchings, S. Jarpe, K.T. Nihei, and M. Schoenball (2020), Seismic Imaging of Spatial- and Temporal Heterogeneity of a Geothermal Reservoir Using a Cost-Effective Dense Seismic Network, *Proceedings, 45th Workshop on Geothermal Reservoir Engineering, Stanford University*, Stanford, California, February 10-12, 2020, SGP-TR-215.

Gutenberg, B., Richter, C. F., 1956. Magnitude and Energy of Earthquakes. Annali di Geofisica, 9: 1–15.

Hartline, C.S., M.A. Walters and M.C. Wright, C.K. Forson and A.J. Sadowski, (2015), Three-dimensional structural model building, induced seismicity analysis, drilling analysis, and reservoir management at The Geysers geothermal field, Northern California, GRC Transactions, 39, 603-614.

Hartline, C.S., M.A. Walters and M.C. Wright, (2016), Three-Dimensional Structural Model Building, Induced Seismicity Analysis, Drilling Analysis and Reservoir Management at The Geysers Geothermal Field, Northern California, PROCEEDINGS, 41st Workshop on Geothermal Reservoir Engineering, Stanford University, Stanford, California, February 22-24, 2016, SGP-TR-209, pp. 1-12.

Hartline, C.S., M.A. Walters, and M.C. Wright, (2019), Three-Dimensional Structural Model Building Constrained by Induced Seismicity Alignments at The Geysers Geothermal Field, Northern California. GRC Transactions, 43, 24 p.

Hearn Jr., B.C., McLaughlin, R.J., and Donnelly-Nolan, J.M., (1988), Tectonic framework of the Clear lake basin, California, Geological Society of America Special Paper, 214, 9-20.

Hutchings L., A. Singh, B. Bonner, S. Jarpe, P. Jeanne, H. Philson, and K. Boyle, (2019), Rock Physics Analysis for Reservoir Properties from Tomographic Images from Micro-earthquakes Recordings, J. Geophys. Res., submitted.

Kjartansson, E., (1979), Constant Q - wave propagation and attenuation, J. Geophys. Res., 84, 9, 4,737-4,748, https://doi.org/10.1029/JB084iB09p04737.

Ludwin, R.S., V. Cagnetti, and C.G. Bufe, (1982), Comparison of seismicity in The Geysers geothermal area with the surrounding region, Bull. Seism. Soc. Am., 72, 3, 863–871.

Majer E.L. and J.E. Peterson, 2007, Impact of Injection on Seismicity at The Geysers, California Geothermal Field, Int. J. Rock Mech. & Min. Sci., 44, 1079-1090.

Masuda T., (1988), Corner frequencies and Q values of P waves by simultaneous inversion technique, Sci. Rep. Tohoku Univ. Ser. 5 Geophys., 31, 101–125.

Mavko, G., T. Mukerji, J. Dvorkin, 1998, The Rock Physics Handbook: Tools for Seismic Analysis of Porous Media, Cambridge University Press, p. 339.

McLaughlin, R.J. (1981), Tectonic setting of pre-Tertiary rocks and its relation to geothermal resources in the Geysers-Clear Lake area, U.S. Geological Survey Professional Paper, 1141, 3-23.

MIT-led interdisciplinary panel, (2006), The Future of Geothermal Energy – Impact of Enhanced Geothermal Systems (EGS) on the United States in the 21st Century, ISBN:0-615-11746.

Moos D. and M. Zoback, (1983), In Situ Studies of Velocity in Fractured Crystalline Rocks, J. Geophys. Res., 88, B3, doi:10.1029/JB088iB03p02345.

Oppenheimer, D.H., (1986), Extensional tectonics at The Geysers geothermal area, California, Journal of Geophysical Research, 91, B11, 11463-11476.

Podvin, P., and I. Lecomte, (1991), Finite difference computation of travel times in very contrasted velocity models: A massively parallel approach and its associated tools, *Geophys. J. Int.*, 105, 271–284.

Stacey, F.D., M. T. Gladwin, B. McKavanagh, A.T. Linde, L.M. Hastie, (1975), Anelastic damping of acoustic and seismic pulses, Geophys. Surv., 2, 2, 133–151.

Stimac, J., Goff, F. and Hearn, B.C., (1992), Petrologic considerations for hot dry rock geothermal site selection in the Clear Lake region, California", Geothermal Resources Council Meeting.

Thurber, C. H., (1983), Earthquake locations and three-dimensional crustal structure in the Coyote Lake area, central California, J. Geophys. Res., 88, 8226–8236.

Toomey, D.R., G. R. Foulger, (1989), Tomographic inversion of local earthquake data from the Hengill - Grensdalur Central Volcano Complex, Iceland, J. Geophys. Res., 94, 12, 17,497-17,510.

Waldhauser, F. and W.L. Ellsworth, (2000), A Double-Difference Earthquake Location Algorithm: Method and Application to the Northern Hayward Fault, California, Bull. Seism. Am., 90, 1353-1368.

Zhang, H., and C.H. Thurber, (2003), Double-Difference Tomography: The Method and Its Application to the Hayward Fault, California, Bul. Seism. Soc. Am., 93, 1875–1889.

Zhu, W., and G.C. Berosa, (2019), PhaseNet: a deep-neural-network-based seismic arrival-time picking method, Geophys. J. Int. (2019) 216, 261–273.

Zucca, J.J., L.J. Hutchings, and P.W. Kasameyer, (1994), Seismic Velocity and Attenuation Structure of the Geysers Geothermal Field, California, Geothermics, 23, 111-126.

APPENDIX A:
Conversion of Seismic Velocities to Elastic Moduli

The spatial correlations between velocities, steam production and water injection in the last section were investigated for the strongest velocity and Vp/Vs anomalies only. However, it is important to systematically investigate all possible spatial correlations between Vp/Vs, the underlying elastic moduli and available steam production and water injection data. Therefore, the elastic parameters were first determined using published relationships between rock densities and P-wave velocities. Two empirical relationships by Brocher (2005) and Gardner et al. (1974) were investigated. Brocher's relationship (Brocher, 2005) is given by equation (1), which is a representation of the by the Nafe–Drake curve

$$\rho = 1.6612 * V_p - 0.4721 * {V_p}^2 + 0.0671 * {V_p}^3 - 0.0043 * {V_p}^4 + 0.000106 * {V_p}^5, \quad (1)$$

while Gardner's relationship (Gardner et al., 1974) is given by

$$\rho = 0.23 * {V_p}^{0.25}. \quad (2)$$

In both equations ρ is the rock bulk density and Vp the P-wave velocity. The relationships in equations (1) and (2) are presented in Figure A-1 for the P-wave velocity interval observed at The Geysers. Through comparison to laboratory measurements of the bulk density of The Geyser's rocks (e.g., Boitnott, 1995; Boitnott and Boyd, 1996), it was concluded that Gardner's relationship is the better fit for this reservoir. Subsequently, the density values were derived from the P-wave velocities estimates, which in turn yielded bulk and shear modulus as well as the Lamé parameter using P- and S-wave velocities. The availability of elastic parameter enables studying the physics of the reservoir on a fundamental level.

Figure A-1: Density P-Wave Relationship

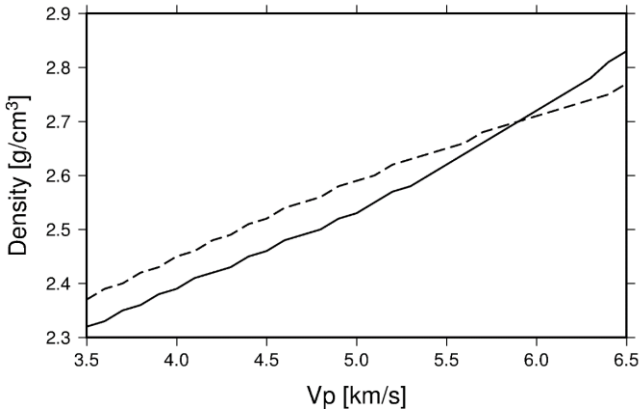

Density as a function of P-wave velocity after Brocher (2005; solid curve) and after Gardner (1974, dashed curve).

Source: Lawrence Berkeley National Laboratory